PNAS RESEARCH ARTICLE | NEUROSCIENCE

Spatial coding in the hippocampus and hyperpallium of flying owls

Arpit Agarwal[a], Ayelet Sarel[b], Dori Derdikman[a], Nachum Ulanovsky[b], and Yoram Gutfreund[a,1]

Edited by György Buzsáki, New York University Grossman School of Medicine, New York, NY; received July 22, 2022; accepted December 9, 2022

The elucidation of spatial coding in the hippocampus requires exploring diverse animal species. While robust place-cells are found in the mammalian hippocampus, much less is known about spatial coding in the hippocampus of birds. Here we used a wireless-electrophysiology system to record single neurons in the hippocampus and other two dorsal pallial structures from freely flying barn owls (*Tyto alba*), a central-place nocturnal predator species with excellent navigational abilities. The owl's 3D position was monitored while it flew between perches. We found place cells—neurons that fired when the owl flew through a spatially restricted region in at least one direction—as well as neurons that encoded the direction of flight, and neurons that represented the owl's perching position between flights. Many neurons encoded combinations of position, direction, and perching. Spatial coding was maintained stable and invariant to lighting conditions. Place cells were observed in owls performing two different types of flying tasks, highlighting the generality of the result. Place coding was found in the anterior hippocampus and in the posterior part of the hyperpallium apicale, and to a lesser extent in the visual Wulst. The finding of place-cells in flying owls suggests commonalities in spatial coding across mammals and birds.

navigation | place-cells | birds | Wulst | wireless neural logger

Significance

Birds travel long distances and navigate in the air as well as on the ground, providing novel and exciting avenues for research on spatial cognition. The brain mechanisms underlying spatial navigation in birds are yet to be discovered. It is hypothesized that the hippocampus in birds, like its mammalian homologue, plays a central role in coordinating spatial behaviors such as navigation, memory, and spatial coordination. We recorded from single neurons in pallial areas of barn owls, including the hippocampus, while they fly between targets. We found neurons that code the direction of flight and the location of the owl in-flight. These results provide unique comparative and evolutionary insights into the coding of space across birds and mammals.

A striking feature of the hippocampal formation of rodents and other mammalian species is the robust neural representation of space by spatial neurons such as place cells, grid cells, and head-direction cells (1–5). These cells are thought to form the substrate for spatial memory and spatial perception in mammals (6–8). An important open question is to what extent similar cells can be found in the brains of other, nonmammalian species, such as birds.

The avian (bird) hippocampal formation (Hp) lies in the posterior medial part of the pallial hemisphere, immediately below the dorsal surface of the brain and above the lateral ventricle (9–14). Directly anterior to the Hp extends the hyperpallium, considered to be a homologue of the mammalian neocortex (15–17). However, the cytoarchitecture of the Hp and the hyperpallium is noticeably different from their mammalian homologues (9, 17). The hippocampal formation is subdivided into a dorsolateral (DL), dorsomedial (DM), and a ventral V-shaped area (14, 18). The hyperpallium is subdivided into four laminae: hyperpallium apicale (HA), interstitial hyperpallium apicale (IHA), hyperpallium intercalatum (HI), and hyperpallium densocellulare (HD) (19). The central part of the hyperpallium includes a primary visual area known as visual Wulst (20). Lesion studies and immediate early gene activation suggest that the Hp and the hyperpallium play central roles in spatial cognition (13, 21–25).

Reports on single-unit activity in the Hp of avian species portrayed diverse results: In quails, head-direction cells were found, but no place-cells (26). In walking pigeons, studies reported multi-field neurons and cells that code locations near rewards and/or the direction toward rewards (27–30). In zebra finches, relatively few place-cells were found, restricted to the anterior part of the Hp (31). In a specialized food-caching bird (tufted titmouse) numerous and robust place cells were found during walking/hopping (31). The seemingly diverse spatial coding across avian species calls for further exploration.

Here, we studied the neurobiology of spatial memory in barn owls. Barn owls are central-place foragers—nocturnal hunters which can self-localize themselves very well even in extremely low light levels (32, 33). While barn owls were extensively studied in sensory neuroscience due to their excellent hearing and vision (34, 35), their hippocampal formation was never studied with electrophysiology.

To this end, we implanted tetrode microdrives in three areas of the dorsal pallium—including in the hippocampal formation—and used a lightweight wireless-electrophysiology system to record single neurons from owls, as they were flying back and forth between two perches at opposite sides of a room, or flying in a search task between four perches. We found a plethora of spatially modulated neurons, including place cells: neurons that

Author affiliations: [a]Department of Neurobiology, Rappaport Research Institute and Faculty of Medicine, Technion, Haifa 3525428, Israel; and [b]Department of Brain Sciences, Weizmann Institute of Science, Rehovot 7610001, Israel

Author contributions: A.A., D.D., N.U., and Y.G. designed research; A.A. and Y.G. performed research; A.A. and Y.G. analyzed data; A.S. developed experimental set-up; and A.A., A.S., D.D., N.U., and Y.G. wrote the paper.

The authors declare no competing interest.

This article is a PNAS Direct Submission.

[1]To whom correspondence may be addressed. Email: yoramg@technion.ac.il.

This article contains supporting information online at https://www.pnas.org/lookup/suppl/doi:10.1073/pnas.2212418120/-/DCSupplemental.

Published January 24, 2023.

fired when the owl flew through a spatially restricted region (place field) in one direction—and often fired differently in the other direction. These various spatially modulated cells were found in the anterior part of the hippocampus (Hp) and in the neighboring posterior part of the hyperpallium apicale (HA_p), but to a much lesser extent in a more central part of the hyperpallium—the visual Wulst—a region considered to be a homologue of the visual cortex (36). This study thus reveals a robust spatial representation in the owl's brain, including spatially localized place cells.

Results

Previous electrophysiological and lesion studies in birds suggested that the anterior Hp is involved in spatial representation and spatial cognition (21, 31, 37). Therefore, in this study we searched for spatial coding in the anterior Hp and in the neighboring posterior region of the hyperpallium apicale (HA_p). To compare with results from a well-characterized primary visual area, we also recorded in the central lateral part of the HA, a retinotopically organized visual area known as the visual Wulst (20, 36). In the initial task—flying back and forth between two perches—we recorded 821 well-isolated single units from six barn owls: 352 from Hp, 376 from HA_p, and 93 from the visual Wulst (*SI Appendix*, Table S1). Spike-shapes tended to cluster into two groups based on spike width (*SI Appendix*, Fig. S1), reminiscent of the distinction between putative inhibitory and excitatory neurons in rodents and birds (31, 38). In the HA_p and possibly Hp, even three groups were observed. However, place coding was detected in all groups (*SI Appendix*, Fig. S1), and therefore below we analyzed all cells together.

Spatially Modulated Cells in the Hp. To target the anterior Hp, we directed the tetrodes 4 mm anterior to the cerebellum edge and 2 to 3 mm lateral from the midline (Fig. 1*A*, *Top*). Recordings were limited to 400–1500 μ below the brain surface. A reconstructed tetrode-track showed that these coordinates yielded a penetration that was 2.7 mm medial to the lateral tip of the lateral ventricle (marked by the black arrow in Fig. 1*A*, *Bottom*), in an area considered well within the hippocampal formation (18, 39) (*SI Appendix*, Fig. S2).

Barn owls tend to fly from one standing position to another in direct trajectories, and do not cover small spaces in volumetric flight like bats, or some other species of birds do (40). Therefore, in our experiments, we started by exploring neuronal firing during a back-and-forth flight between two perches located on opposite walls, separated by 4 m (see *Materials and Methods*). During each ~20-min recording session, the owls flew 30 to 45 flights in each direction, with highly reproducible trajectories that formed a 1D "flyway" (Fig. 1*B* and *SI Appendix*, Fig. S3 and Movies 1 and 2)—allowing to statistically compare the firing-rates between flight directions or between perch locations. In the example session shown in Fig. 1 *B–F*, the owl spent about 90% of the session standing on either of the perches and about 10% of the time flying between perches (Fig. 1*C*). Firing rates of the example neuron shown in Fig. 1 *B–F* were higher during flight compared with standing (Fig. 1*C*, red curve). Interestingly, during flight, most of the firing of this neuron occurred in a place-field located between 1.5 and 3 m from the west wall—but only during westbound flights. During eastbound flights, the same neuron fired almost no action potentials (Fig. 1 *D–F*). In this neuron, there were significant differences in firing-rates between perching versus flying and between westbound-flights versus eastbound-flights (bootstrap, $P < 0.001$). Importantly, the neuron exhibited significant place-tuning during westbound flights ($P < 0.001$, compared with spike-shuffling), and the spatial information (*SI Appendix*) was 0.41 bits/spike, i.e., this was a significant place-cell. Additional examples of significant hippocampal place cells are shown in Fig. 1*G* and *SI Appendix*, Fig. S4.

Overall, we identified in Hp recordings three spatially related parameters that significantly modulated the firing rates of the cells: 1) Place tuning: Selectivity to a specific position in the flight path, in at least one of the directions. We used the spatial information to quantify the place-tuning of the neurons during flight. Out of the 352 cells recorded in Hp, 167 (47%) were significantly place-tuned in at least one direction (rigid circular spike-shuffling, $P < 0.01$). To avoid inclusion of cells with low spatial information but whose spatial modulation was nevertheless significant due to a high firing-rate, we used an additional criterion: we required spatial information >0.3 bits/spike for a significant place-tuned cell to be included in our population of analyzed place-cells. Ninety six neurons (27%) passed this criterion for place cells ($P < 0.01$ and SI > 0.3 bits/spike). Among these, 73 cells were significantly place-tuned during westbound flights and 53 cells during eastbound flights (see examples in Fig. 1 *E* and *G* and *SI Appendix*, Fig. S4). 2) Directionality: Flying toward the east versus flying toward the west. Out of the 352 cells recorded in Hp, 117 cells (33%) exhibited significant directionality (bootstrap, $P < 0.01$; examples in Fig. 1 *E* and *G* and *SI Appendix*, Fig. S4): 37 cells significantly preferred eastbound flights and 80 cells significantly preferred westbound flights. 3) Selectivity to standing on the east perch versus standing on the west perch. Out of the 352 cells recorded in Hp, 144 cells (41%) exhibited significant selectivity to one of the perches: 72 cells significantly preferred the west perch and 72 cells significantly preferred the east perch (bootstrap, $P < 0.01$; examples in Fig. 2*A*). The three types of spatial modulation (place tuning, directionality, and perch selectivity) were intermixed: 31% of the spatially modulated cells displayed more than one type of selectivity, with some cells' firing-rate significantly modulated by all three types (n = 25; Fig. 2*B*). Among the cells that showed both significant directionality and significant perch sensitivity, there was no significant correlation between the location of the preferred perch and the preferred flight direction (Fig. 2*C*, main; Pearson r = 0.26, $P = 0.1$). However, for absolute values of discrimination indices (DIs) a significant correlation was found between the DIs of perch and flight-direction (Fig. 2*C*, *Inset*; r = 0.57, n = 66, $P < 0.001$). Thus, cells with large DIs for flight direction tended to have also large DIs for perch, irrespective of the direction.

Across the population of recorded neurons, the normalized differences between the firing-rates during westbound and eastbound flights (flight DIs; see *SI Appendix*, Eq. **S2**) ranged from cells strongly preferring westbound flights to cells strongly preferring eastbound flights, with more cells preferring the former (Fig. 2*D*, *Left*; 171 negative DIs compared with 105 positive DIs; Sign test, $P < 0.001$). Perch preferences varied from west perch preferring cells to east perch preferring cells, with a roughly equal representation of both sides (Fig. 2*D*, middle panel; 182 negative DIs and 170 positive DIs). In addition, 54 cells showed significantly higher firing-rates during flight compared with when standing on the perch, and 85 cells showed the opposite (bootstrap, $P < 0.01$; Fig. 2*D*, *Right*).

To examine the spatial distribution of the significant place-fields during flight, we computed the smoothed 1D firing-rate curves (rate maps) for all the significant place-cells (example in Fig. 2*E*, black curve). At the population level, the place fields covered the entire flyway, with an over-representation of the regions near the perches (Fig. 2*F*; rate maps were sorted according to the position of the peak firing-rate—separately for the two directions). The

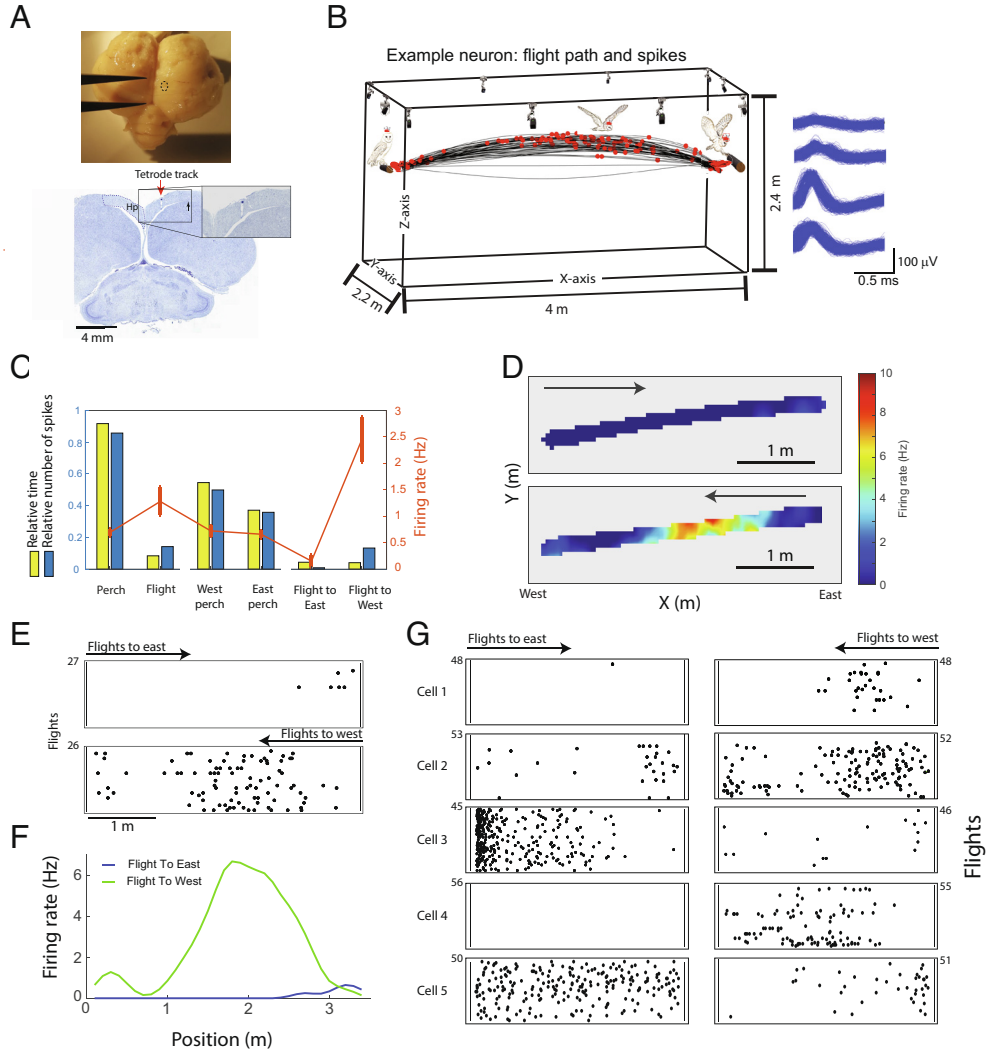

Fig. 1. Recording location and example place cells in the hippocampus (Hp). (*A*) An upper view of the brain of owl DK after removal. The dashed oval marks the position of the craniotomy. The caliper is set to 5 mm. The lower image shows a Nissl-stained coronal section of the above brain showing the tetrode track (red arrow); the dashed line outlines the hippocampal formation (Hp) in the opposite hemisphere. Black arrow in the histological section points to the lateral tip of the lateral ventricle, which is a putative estimation of the lateral border of Hp. (*B–F*) Results from one example neuron. (*B*) The flight trajectories of an example recording session (black; shown are both flight directions). Red dots represent the spikes of a single unit whose spike shapes are shown in the *Inset* on the *Right*. The flights are superimposed on an illustration of the flight room and cameras. (*C*) The relative time (from the total time of the session) and the relative number of spikes (from the total number of spikes fired by this example neuron) are shown for each of the six possible behavioral states: standing on a perch, flying, standing on the west perch, standing on the east perch, flying eastward, and flying westward. The red curve depicts the firing rates in the above six different states (mean ± SE). (*D*) A 2D firing-rate map of the cell (*Top* view, XY) drawn separately for westbound flights (*Bottom*) and eastbound flights (*Top*). Arrows mark the flight direction. Colors denote the firing rate. Pixels in which the owl did not visit are shown in gray. (*E*) Raster plots showing the spike times along the flight path, for the same cell. The upper raster shows all eastbound flight and the lower raster all westbound flights. Each row is a different flight; the number of flights in each direction is indicated on the Y-axis. The X-axis, here and in all examples that follows, is the X-position in the room. (*F*) The smoothed firing-rate map of the neuron as a function of position, shown separately for eastbound flights (blue curve) and westbound flights (green curve). (*G*) Raster plots for five additional example neurons during flights to the east (*Left* column) and to the west (*Right* column); the number of flights is indicated on the Y-axis.

rate-maps for the two different directions from the same cell were not correlated, in most cases (*SI Appendix*, Figs. S4 and S9 *A–C*)—and only 30 cells out of the 96 place cells were significantly spatially tuned in both directions.

To assess the stability of the place-fields, we computed the Pearson correlation coefficient between 1D firing-rate maps that were constructed separately for the first versus second half of the session (Fig. 2*G*, blue; computed for all flight-directions that exhibited significant place-tuning, n = 127; note that a place-cell can be place-tuned in both directions or only in one direction, hence the number of place-tuned directions is larger than the number of place-cells). The correlations were highly positive (median Pearson correlation coefficient: r = 0.65,) and significantly higher than the distribution of cell-wise shuffled correlations (Fig. 2*G*, black curve; median Pearson correlation for the shuffle: r = 0.01; Kolmogorov–Smirnov test comparing data to shuffle: $P < 0.0001$)—indicating stability of the place-tuning. To assess the stability of the neurons' directional preferences over time, we divided the session into two halves and analyzed the DIs between flight directions and between the two perches. This analysis included only cells which showed a significant flight-direction preference (n = 117) or perch-location preference (n = 144). DIs of flight direction and perch location were significantly and highly correlated between the two halves of the session (flight direction preference: Pearson r = 0.94, $P < 0.0001$; perch preference: Pearson r = 0.93, $P < 0.0001$; Fig. 2 *H* and *I*). Overall, spatial preferences in Hp were maintained stable during the experimental session.

Spatially Modulated Cells in the HA_p. In a second set of experiments, we targeted the posterior part of the hyperpallium

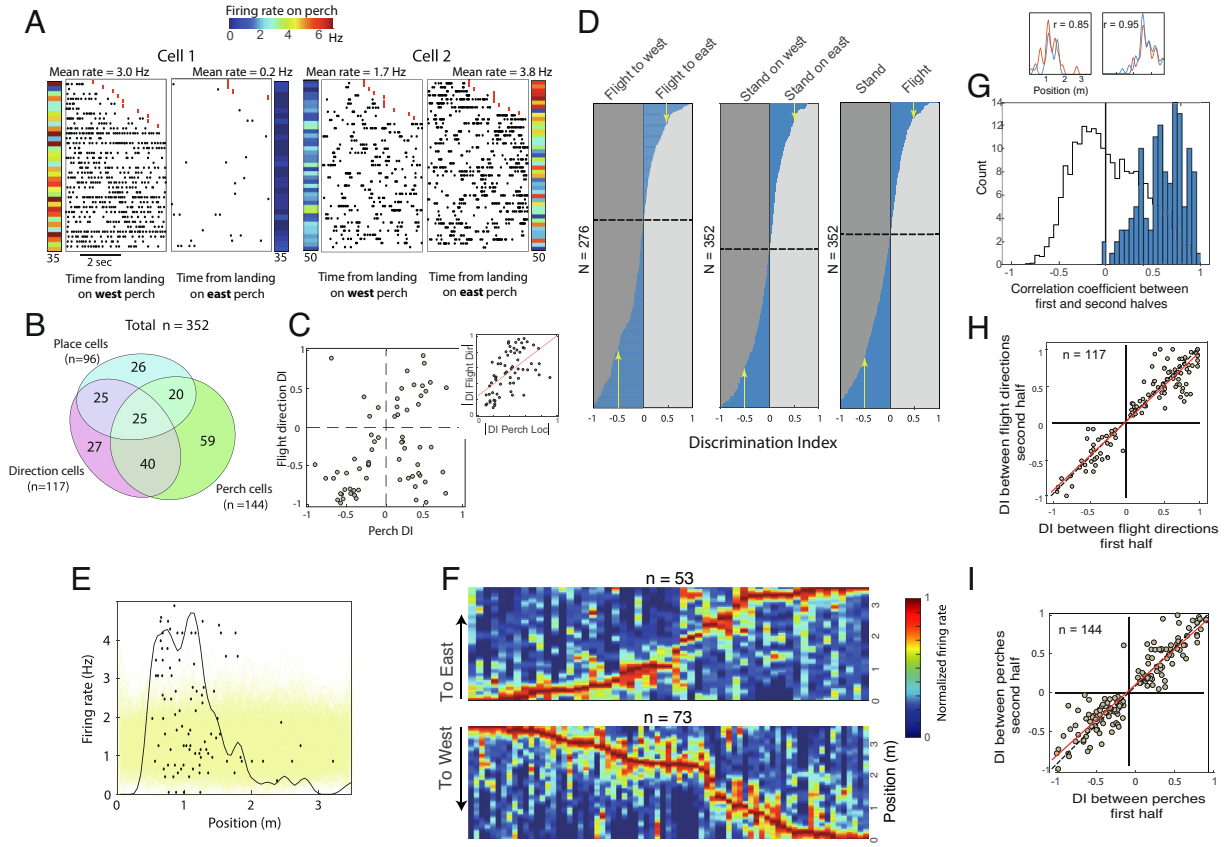

Fig. 2. Spatial modulation of neuronal responses in the Hp. (*A*) Two example neurons showing significant asymmetric firing between the two perches. Black dots show spike-times relative to the time of landing on the west perch (*Left* raster) or on the east perch (*Right* raster). Shown are the first 5 s after landing; in trials where the owl stayed on the perch less than 5 s, the time of leaving the perch is marked by a red tick. Flights are sorted according to the time on perch. Spikes during flight (to the *Right* from the red ticks) were not displayed. The color-bars on the *Left* and *Right* sides of the rasters designate the mean firing rates for each trial on the west and east perches, respectively. (*B*) Venn-diagram showing the relations between three types of spatial modulations (place-tuning during flight, direction selectivity, and perch selectivity) in the population of neurons from the Hp. (*C*) A scatterplot showing the relationship, within cells, between the perch discrimination index (DI) and the flight-direction discrimination index. The inset shows the relationship between the absolute values of the perch DIs versus the absolute values of the direction DIs. (*D*) Histograms showing the DIs for flight direction (*Left*), standing perch position (*Middle*) and standing versus flying (*Right*). X-axis, discrimination index; Y-axis, cells: sorted from the most negative DI to the most positive DI. The horizontal dashed line indicates the zero DI. The number of cells in each graph is shown on the *Left*. Vertical arrows mark cells with DI > 0.5 in both directions. (*E*) Example cell showing raster (black dots) and 1D firing-rate map (black curve) for one flight-direction. The yellow curves show 100 firing-rate curves generated from rigidly shuffling the spike trains in-flight in the same flight-direction. (*F*) Color plots of the smoothed firing-rate maps, for all significant place-cells in the Hp. Each column depicts a single firing-rate map, normalized by the peak firing-rate of the neuron. Results are shown separately for flights to west (*Bottom* plot) and flights to east (*Top* plot). Curves are sorted from *Left* to *Right* according to the position of the peak firing. The arrows mark the beginning of flight and the flight direction. (*G*) Distribution of Pearson correlation coefficients between the 1D firing-rate maps generated from the first and second halves of the session (blue bars). Firing-rate maps from both directions are pooled. The black curve is the cell-shuffling distribution of the Pearson correlations of the first half from neuron *i* versus the second half from neuron *j*, from all neuron-pairs such that $i \neq j$. *Inset*: two example neurons showing the 1D firing-rate maps for the first half of the session (red lines) and second half of the session (blue lines). Pearson correlation coefficient between the red and blue curve is indicated for each example. (*H*) The DIs between flight directions, calculated from the first half of the session, are shown versus the DIs calculated from the second half of the session. Only cells that significantly discriminated between flight directions were included in this graph. Dashed line, identity-diagonal; red line, linear-regression. (*I*) Same as in *G* but showing the DIs between perches in the first half versus the second half of the session.

apicale (HA_p)—located immediately anterior and lateral to the hippocampus. The tetrodes were implanted 5 to 6 mm anterior from the cerebellum and 2.5 to 3.5 mm lateral from the midline (Fig. 3*A*, *Top*). We used the lateral tip of the lateral ventricle (black arrows in Fig. 1*A*–*Bottom* and Fig. 3*A*-*Bottom*) as a histological landmark to mark the putative boundary between the Hp and HA_p (39, 41). In the more anterior section in Fig. 3*A*, this tip is closer to the midline compared with Fig. 1*A* (*SI Appendix*, Fig. S2). A reconstructed tetrode-track obtained in one of the owls showed that these coordinates resulted with a penetration that was 1.7 mm lateral from the lateral tip of the lateral ventricle (Fig. 3*A*, *Bottom*), in an area presumed to be in the posterior part of the hyperpallium (18, 39). Since we limited our recordings to about 1.5 mm below the brain surface, the recorded neurons are most likely to be in the posterior hyperpallium apicale (HA_p) (19). However see *Discussion* for a possibility that the putative recording sites in HA_p are, in fact, in an extended rostral and lateral part of Hp.

In the HA_p, we found the same three types of spatially modulated neurons that we found in the Hp. Surprisingly, however, a larger percentage of spatially modulated neurons were encountered in the HA_p as compared with the Hp: 1) Place tuning: Out of 376 cells, the firing rates of 280 cells (74%) were significantly modulated by the position along the flight trajectory in at least one direction (spike-shuffling statistics, 99% percentile: i.e., $P < 0.01$). Among these, 178 cells (48%) passed our additional criterion for place-cells (Spatial Information > 0.3 bits/spike; examples in Fig. 3*B* and *SI Appendix*, Fig. S5): 117 cells were significantly spatially tuned during westbound flights and 125 during eastbound flights. 2) Directionality: Out of 376 cells, 157 cells (42%) exhibited significant directionality: 73 cells significantly preferred

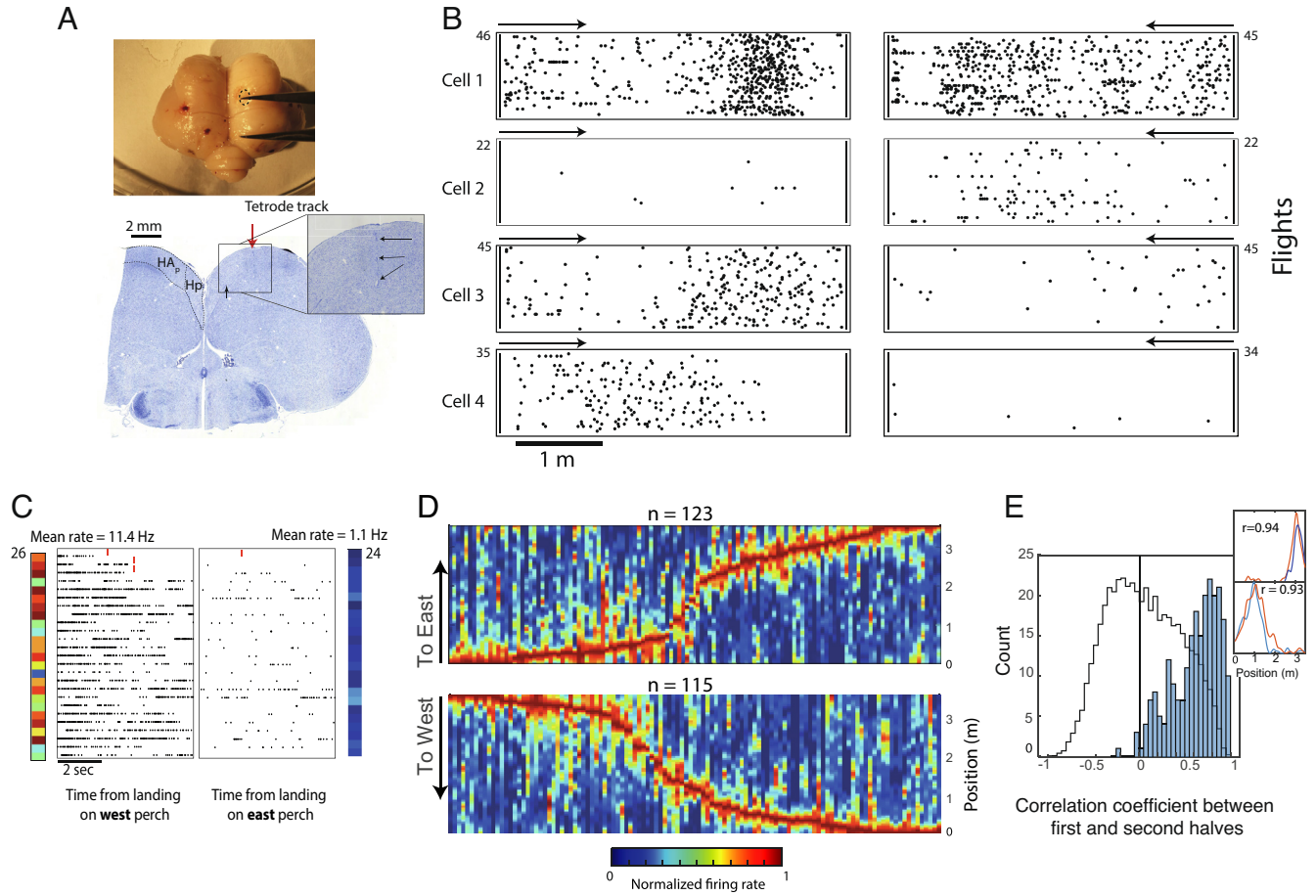

Fig. 3. Spatial tuning in the posterior hyperpallium apicale (HA_p). (*A*) The brain of owl TLV1 after removal. The dashed oval marks the position of the craniotomy. The caliper is set to 5 mm. The lower image shows a Nissl-stained coronal section of the above brain. The tetrode track is marked by the red arrow. Arrows in *Inset* point to scars from the three focal electrolytic lesions made along the track. The black arrow points to the lateral tip of the lateral ventricle. The dashed lines outline the putative borders of the hippocampal formation (Hp) and the HA. (*B*) Raster plots of four example place-cells showing spike occurrences along the flights eastward (*Left* plots) and flights westward (*Right* plots). Arrows indicate the starting position and direction of flight for each of the plots. The numbers on the Y-axis indicate the number of flights. (*C*) An example of a perch-selective cell in HA_p. The rasters show the spike times relative to landing on the west perch (*Left* raster) and the east perch (*Right* raster). Plotted as in Fig. 2*A*. (*D*) Color plots of the smoothed firing rate curves from all place-cells in HA_p (Spatial Information larger than 99% of the shuffles and larger than 0.3). Each column designates a single firing-rate map, separately for flights to west (*Bottom*) and flights to east (*Top*). Curves are sorted from *Left* to *Right* according to the position of the peak firing. The arrows mark the beginning of flight and flight direction. (*E*) Distribution of Pearson correlation coefficients between the 1D firing-rate maps generated from the first half versus second half of the session (blue bars). Black curve shows the cell-shuffling distribution of the Pearson correlations of the first half from neuron *i* versus the second half from neuron *j*, from all neuron-pairs such that $i \neq j$. *Insets*: two examples neurons, showing the 1D firing-rate maps for the first half of the session (red lines) and second half of the session (blue lines). Pearson correlation coefficient between the red and blue curves are indicated for each example.

eastbound flights and 84 significantly preferred westbound flights (bootstrap statistics, $P < 0.01$; examples in Fig. 3*B* and *SI Appendix*, Fig. S5). 3) *Perch selectivity:* When standing on the perch, 165 out of 376 cells (44%) exhibited significant selectivity to one of the perches (example in Fig. 3*C*): 81 cells significantly preferred the east perch and 84 cells the west perch (bootstrap statistics, $P < 0.01$).

In HA_p, a substantial overlap between the three types of spatial modulation was observed, with 47 cells exhibiting significant modulation by all three parameters (place-tuning, directionality, and perch-preference; *SI Appendix*, Fig. S6*A*). Again, there was no significant correlation between the preferred perch side and the preferred flight direction (*SI Appendix*, Fig. S6*B*; Pearson r = 0.17, n = 81, $P = 0.1$).

In both brain regions (Hp and HA_p) a substantial number of cells distinguished between flight directions and/or perch positions, with high discrimination values (Fig. 2*D* and *SI Appendix*, Fig. S6*E*). In the HA_p, no significant bias for flight direction was observed (165 positive DIs versus 174 negative DIs; Sign test, $P = 0.74$). In both Hp and HA_p, the place-fields exhibited overrepresentation of space at the two ends of the flyway, near the perches (Figs. 2*F* and 3*D*)—as found in rodents and bats near reward zones (42–44). The neural representations of location (place-tuning) were highly stable between the first and second halves of the session (Fig. 3*E*, median Pearson correlation between first versus second half, r = 0.664, n = 238). Likewise, directionality of neural responses during flight, and perch preferences, were maintained stable between the first and second halves of the session (*SI Appendix*, Fig. S6 *C* and *D*; directionality: Pearson r = 0.88, n = 159; perch preference: r = 0.91, n = 167).

Properties of Spatially Modulated Cells in Hp and HA_p. Occasionally, the owls made a U-turn in mid-flight, turning back to land on the perch from which they took off. These events provided an opportunity to examine whether the directional sensitivity is determined by the flight direction per se, independent of the starting position. In the example session shown in Fig. 4*A*, the owl made two U-turns. Action potentials in the U-turn trials were more abundant when the owl was flying westbound, along the preferred direction of the cell (Fig. 4*A*, *Top* panel).

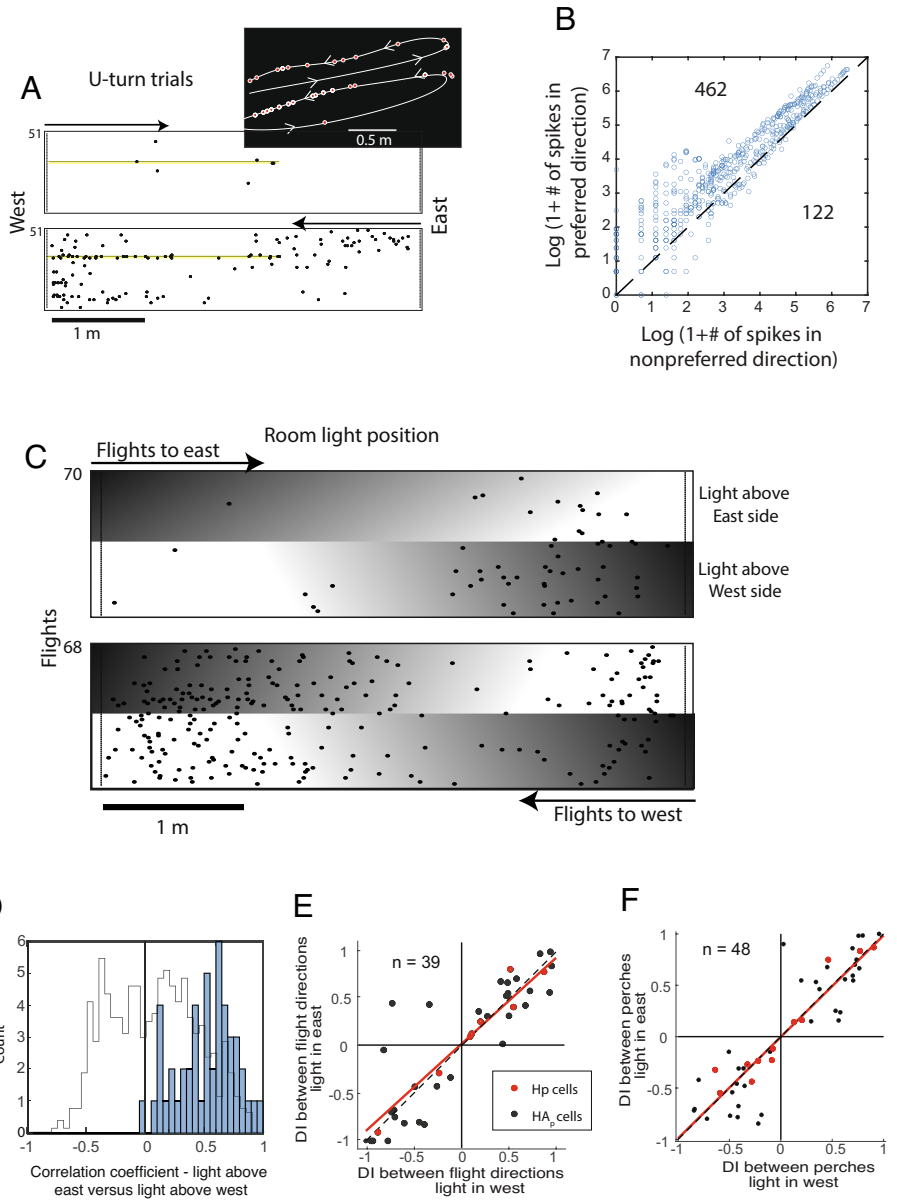

Fig. 4. U-turns and experimental manipulations. (*A*) Raster-plots for an example neuron recorded in HA_p, showing significant preference to westbound flights (*Bottom*) over eastbound flights (*Top*). The yellow and green lines on the rasters mark the two trials in which the owl started on the west perch, made a U-turn in mid-flight, and landed again on the west perch. Inset above (black): *Top* view of the flight trajectories of these two trials. The trajectories were shifted on the Y-axis to separate them for display purposes. Red dots on the trajectories indicate spikes. The arrowheads point to the direction of flight. (*B*) Each dot in the scatter-plot represents a single U-turn trial (data are pooled from all experiments in Hp and HA_p). The Y-axis shows the number of spikes discharged in the preferred direction, and the X-axis the number of spikes in the nonpreferred direction. The number of dots above and below the diagonal (equality line) are indicated. Data are shown on a log–log scale. (*C*) An example of a neuron's firing during flights when the light was above the west perch and then flipped in the middle of the session to the opposite side of the room. The direction of the lighting pattern in the room is indicated by the white-to-black background shading. Bottom raster shows flights to west and top raster flights to east. (*D*) Blue bars: distribution of Pearson correlation coefficients between the 1D firing-rate maps computed for the two parts of the session: light-in-west versus light-in-east. Black curve: the cell-wise shuffled distribution of Pearson correlations between the first and second parts of the session. (*E*) Scatter-plot showing the DIs between flight directions when the light was in the east versus the DIs when the light was in the west. Red dots, cells that were recorded in Hp; blue dots, cells recorded in HA_p. Dashed line, identity-diagonal; red line, linear-regression. (*F*) Same as *E* but showing the DIs between the perches when the light was in the east versus when the light was in the west.

A summary of the spike counts recorded in U-turn trials from all the experiments, shows that the number of spikes discharged when the owl was flying in the preferred direction was significantly larger compared with the number of spikes discharged when the owl was in the opposite direction [Fig. 4*B*; Sign test, $P < 0.0001$; n = 584 (pooled data from Hp and HA_p)]. Thus, the neuronal activity is determined by the instantaneous flight of the owl and not by the takeoff direction.

Next, we examined the effect of lighting conditions on the place-tuning of neurons. The experimental room was normally illuminated by three LED lamps: one at the center, one above the east perch, and one above the west perch. In several of the sessions, we changed the illumination in midsession: in the first half of the session, the arena was illuminated only with the light above the west perch, and in the second half, we switched to illuminating only with the eastern light. This created an asymmetric lighting in the room that was switched to the opposite side in midsession. The switch in lighting-conditions had little effect on the firing pattern of the example cell shown in Fig. 4*C*—and importantly, it changed neither the place-tuning nor the flight-direction

preference. At the population level, the pattern of place-tuning (firing-rate curves) was stable independent of the lighting condition for most of the significant place-cells tested with this manipulation (Fig. 4*D*; median Pearson correlation coefficient: r = 0.58, n = 47 tuning curves from 29 cells). Flight direction preference was not changed in most of the direction-significant neurons, which were tested in this experiment (Fig. 4*E*; Pearson r = 0.87, $P < 0.0001$, n = 39), and the perch preference was also not changed (Fig. 4*F*; Pearson r = 0.86, $P < 0.0001$, n = 48). During the recording sessions, an experimenter was present in the room, adjacent to the south wall, to encourage the owls to fly back and forth (see *Materials and Methods*). Similar to the switch in lighting conditions, spatial coding was maintained fixed, independent of the experimenter's position in the room (*SI Appendix*, Fig. S6 *F–I*).

To explore spatial coding without an experimenter in the room, as well as in a task with multiple flight goals and less stereotypic flight paths, we devised an additional experimental task. In this task four perches were mounted in the room, one on each wall. Owls were trained to receive a food reward from a feeder on one of the perches (see *Materials and Methods*). For the feeder to deliver a reward, the owl had to fly to one designated perch (the rewarding perch) and stand there for 1 s. From there, the owl had 20 s to fly to the feeder to obtain the reward. After every opening of the feeder, the rewarding-perch was randomly reselected with equal probability between the perches. Therefore, the owl had to search for the rewarding perch by flying between the perches. In the example session of Fig. 5*A* (Movie S3) the feeder was on the east wall, and the owl flew spontaneously between perches providing several different flight paths. Remarkably, during flight, this neuron fired only when the owl flew from the east perch to the west perch and only within a restricted place.

In this task (four-perch experiment with a feeder), we recorded 317 single units in the Hp of three owls (*SI Appendix*, Table S1). Eighty cells emitted less than 20 spikes during flight and were

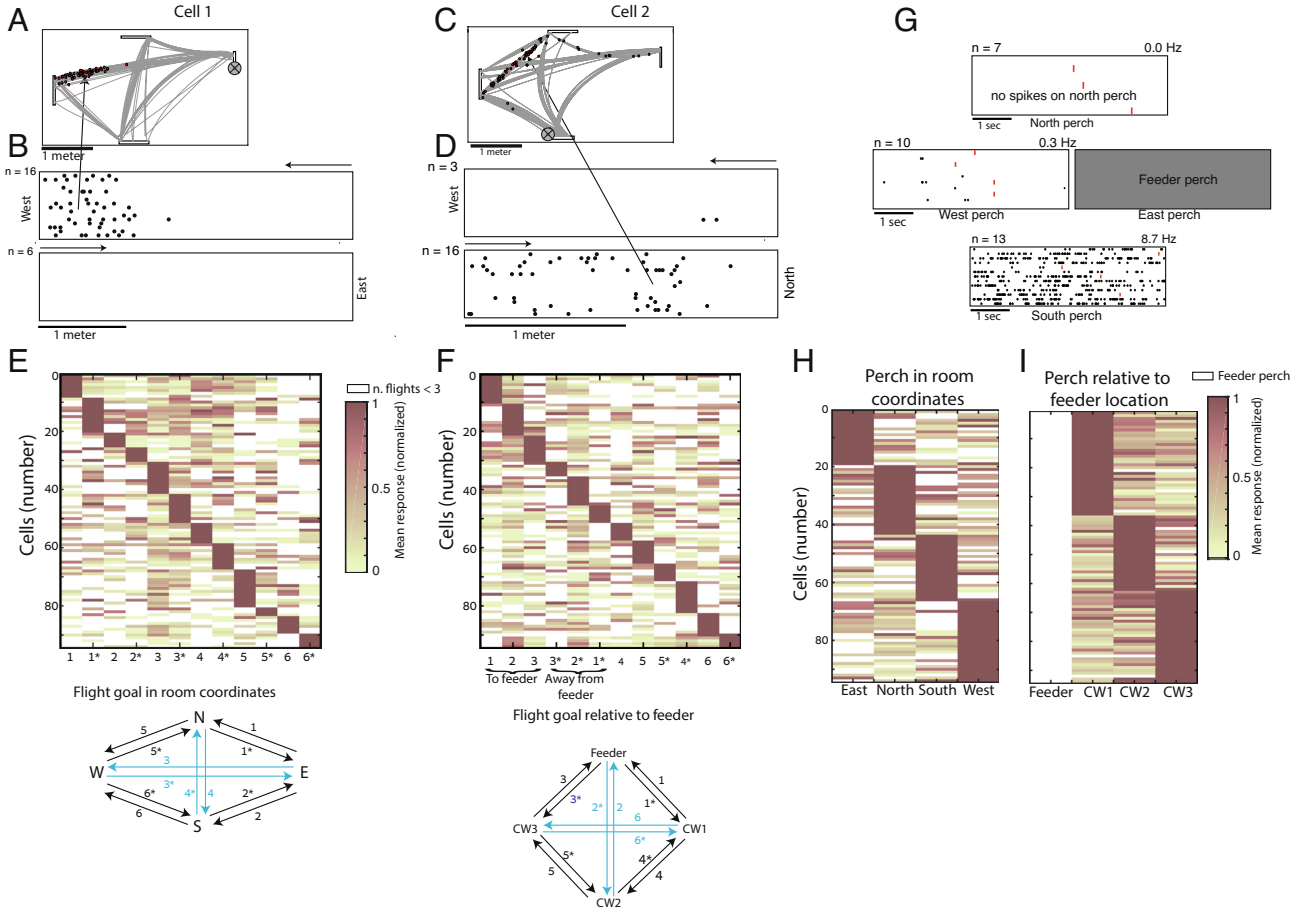

Fig. 5. Spatial responses in experiments with four perches. (*A*) An example of a place-cell recorded in the feeder experiment. *Left* panel shows a 2D upper view of the flight paths (gray lines). Perches are designated by black rectangles. Upper perch is north. Red dots designate occurrences of a single neuron action potentials during flight. Spikes on perches are not shown. The gray circle designates the feeder location. (*B*) Raster plots showing the occurrences of spikes in the east–west flights for the cell in *A*. The upper raster shows all westbound flights and the lower raster all eastbound flights. Each row is a different flight; the number of flights in each direction is indicated on the Y-axis. The arrows mark the beginning and direction of flights. (*C* and *D*). Same as *A* and *B* but showing a different neuron recorded in a different session. (*E*) Normalized mean firing rates during flights are plotted as a function of the flight's position and direction. The diagram below shows the key to flights between north, west, south, and east perches. Each row is a single significant place-cell. Cells were sorted according to the flight with the maximal firing rate, beginning with cells with maximal firing-rate when flying from east to north (*Left* column) and ending with cells with maximal firing-rate when flying from west to south (*Right* column). (*F*) Same as in *E* but cells are organized according to flights relative to feeder location (which changed between sessions). (*G*) Raster plots showing the spikes of one neuron during the first 5 s after landing on the perches. In this session the feeder was on the east perch [the raster for the feeder is not shown (gray) because it was not analyzed in order to avoid biases due to feeding and reward; see *Methods*]. The numbers of visits on each perch and mean firing-rate on each perch are displayed above each raster. Red tics indicate the times the owl left the perch, in trials for which the time on the perch was less than 5 s. (*H*) Mean firing rate on the perch as a function of perch location for all the cells with significant perch preference (Kruskal–Wallis test, $P < 0.01$). Cells are sorted according to the preferred perch. White bars indicate the feeder perch (responses not analyzed on the feeder perch) or a perch visited less than three times. (*I*) Mean firing rate on the perch relative to the feeder location. CW1, first perch clockwise to feeder; CW2, second perch clockwise to feeder (opposite feeder); CW3, third perch clockwise to feeder.

excluded from the analysis. The in-flight 2D rate maps of the remaining 237 cells were analyzed (*SI Appendix*), and revealed that 115 of the cells had spatial information significantly larger than chance (rigid circular spike-shuffling, $P < 0.01$). As in the two-perch experiment, we imposed an additional criterion: Spatial Information >0.3 bits/spike was required for a significant placed-tuned cell to be considered a place-cell. Among the 115 significant cells, 94 passed this criterion. Examples of such place-cells are shown in Fig. 5 *A* and *D* and *SI Appendix*, Fig. S7: these examples showed rich spatial responses, with some cells exhibiting single place-fields while others exhibiting multiple place fields. Notably, separating neural responses to specific flight paths and directions (Fig. 5 *B* and *D* and *SI Appendix*, Fig. S7) revealed neural responses similar in appearance to the neural responses of place cells recorded in our initial experiment in owls flying between two perches: Namely, responses were spatially selective, and responses in one direction were largely different from responses in the opposite direction.

In the population of 94 place-cells that were recorded in the four-perch feeder experiment, place fields were observed in all 12 possible flight paths between the four perches, without a significant bias to any one flight path (Kruskal–Wallis test, $P > 0.05$; Fig. 5*E*). We then examined whether place-field locations are correlated with the feeder location (reward location) by plotting the mean response per flight relative to the feeder's location (Fig. 5*F*). Place fields were observed about evenly in all possible flight paths relative to feeder location (Kruskal–Wallis test, $P > 0.05$). Thus, across the population of place-cells, flights toward the feeder did not elicit more responses as compared with flights toward other perches.

In this experiment, as in the two-perch experiment, some cells were significantly perch-selective (example in Fig. 5*G*). To explore neuronal perch preference, we computed the mean firing rates during the first 5 s of standing on the perches. To eliminate effects of feeding behavior and reward, we excluded from this analyses the feeder perch. The firing rates on the three remaining perches were significantly selective to standing-perch location in 95 cells (Kruskal–Wallis, $P < 0.01$). Among these neurons, cells preferring north, east, south, and west perches were encountered about evenly (Fig. 5*H*; Kruskal–Wallis test, $P > 0.05$). Finally, the distribution of neuronal perch preference was not related to the feeder's location (Fig. 5*I*; Kruskal–Wallis test, $P > 0.05$).

Single-Unit Responses in Visual Wulst. To examine whether the newly found spatial representation in the HA_p is restricted to the posterior part of the HA or is anatomically widespread across the avian hyperpallium, we targeted our recordings in the next experiment to the lateral central part of the hyperpallium. This area, which is called visual Wulst, has been well characterized in barn owls (20, 36, 45). It is a retinotopically organized visual area that is the main recipient of the thalamofugal visual pathway (20, 46, 47). In this location, we recorded in a head-fixed condition neurons with small visual receptive fields (RF, ~5° diameter) at the frontal visual field (Fig. 6*A*). Based on previous mapping, such responses correspond to a location at the lateral central part of the retinotopic visual map in the visual Wulst (36).

We then turned to recording visual Wulst neurons in flight. In total, we recorded 93 single units in the visual Wulst from two owls (*SI Appendix*, Table S1). The average firing-rate during flight was significantly higher than during perching (*SI Appendix*, Fig. S11*A*; *t* test, $P = 0.0076$). Moreover, Firing-rates in the visual Wulst were significantly higher compared with firing-rates in both Hp and HA_p (*t* test, $P < 0.001$), and firing-rates in HA_p were significantly higher than in Hp (*t* test, $P < 0.001$). In the visual Wulst, we also found neurons that significantly discriminated between the two flight directions (32% of the neurons; *SI Appendix*, Fig. S11*B*). However, overall these showed strikingly lower DIs for flight direction as compared with Hp and HA_p: While in Hp and HA_p a substantial number of neurons had high DIs (for illustration, DIs higher than 0.5 are marked by arrows in Fig. 2*D* and *SI Appendix*, Fig. S6*E*), the maximal discrimination index in the visual Wulst was 0.33 for flight-direction (Fig. 6 *B* and *D*)—much lower than in Hp and HA_p. Moreover, unlike in Hp and HA_p, discrimination between perches in the visual Wulst was very scarce (only four cells significantly discriminated between perches). The DIs, both for flight direction and perch position, were significantly smaller in the visual Wulst as compared with Hp and HA_p (Fig. 6 *D* and *E*; Kolmogorov–Smirnov test, $P < 0.001$). In other words, cells that showed substantial differences between firing-rates in different directions or perches were found in Hp and HA_p—but not in the visual Wulst.

In the visual Wulst, 81 out of 93 cells (89%) were significantly modulated by location during flight. From these, only 27 cells (29%) passed our criteria for place cells (spike-shuffling statistics, $P < 0.01$ and spatial information > 0.3 bits/spike). This compares with 27% in Hp and 48% in HA_p (*SI Appendix*, Fig. S11*B*). The place fields size and number of fields per direction were not significantly different from HA_p and Hp (2-way ANOVA, $P > 0.05$; *SI Appendix*, Fig. S10). However, interestingly, the 27 place-cells in the visual Wulst were highly symmetrical between the two flight directions—i.e., the firing pattern in one direction was a mirror image of the firing pattern in the opposite direction (*SI Appendix*, Fig. S9 *G–I* and examples in Fig. 6*C* and *SI Appendix*, Fig. S8). The cumulative distribution of the symmetry indices was significantly more positive in the visual Wulst compared with Hp and HA_p (Kolmogorov–Smirnov test, $P < 0.001$; Fig. 6*F*). The symmetry indices were maintained larger in the visual Wulst compared with Hp and HA_p also when considering all significantly modulated cells, including cells with spatial information smaller than 0.3 (*SI Appendix*, Fig. S11*C*)—indicating that visual Wulst neurons encoded the distance from takeoff or from landing, regardless of flight direction.

Finally, the values of the spatial information were significantly smaller in the visual Wulst compared with Hp and HA_p (Kolmogorov–Smirnov test, $P < 0.001$; Fig. 6*G*; using all neurons with significant spike-shuffling statistics of $P < 0.01$ on place-tuning). The reduced magnitude of place-tuning in the visual Wulst was significant when using two other indices to quantify spatial tuning in hippocampal neurons: sparsity, and selectivity (48) (*SI Appendix*, Fig. S11).

In rodents, the variability of spike-rates across different passes through a place field was shown to often be larger than expected from a Poisson distribution (overdispersion) (49, 50). We therefore analyzed the spike-rate variability of place cells across flights (*SI Appendix*; we used a Normal approximation of the Poisson distribution). Significant overdispersion was found in 73% of the place-cells in Hp, 49% of the place-cells in HA_p and 23% of the place-cells in the visual Wulst (Kolmogorov–Smirnov normality test; $P < 0.05$).

Discussion

Barn owls are nocturnal predators that spend much of the nighttime perching on strategic posts, occasionally leaving the branch to explore for rodents (33, 51). In an enclosed space, they do not spontaneously cover 3D space volumetrically in flight, but rather they naturally tend to fly in straight lines from one standing position to the other (40). Therefore, in our experiments, we

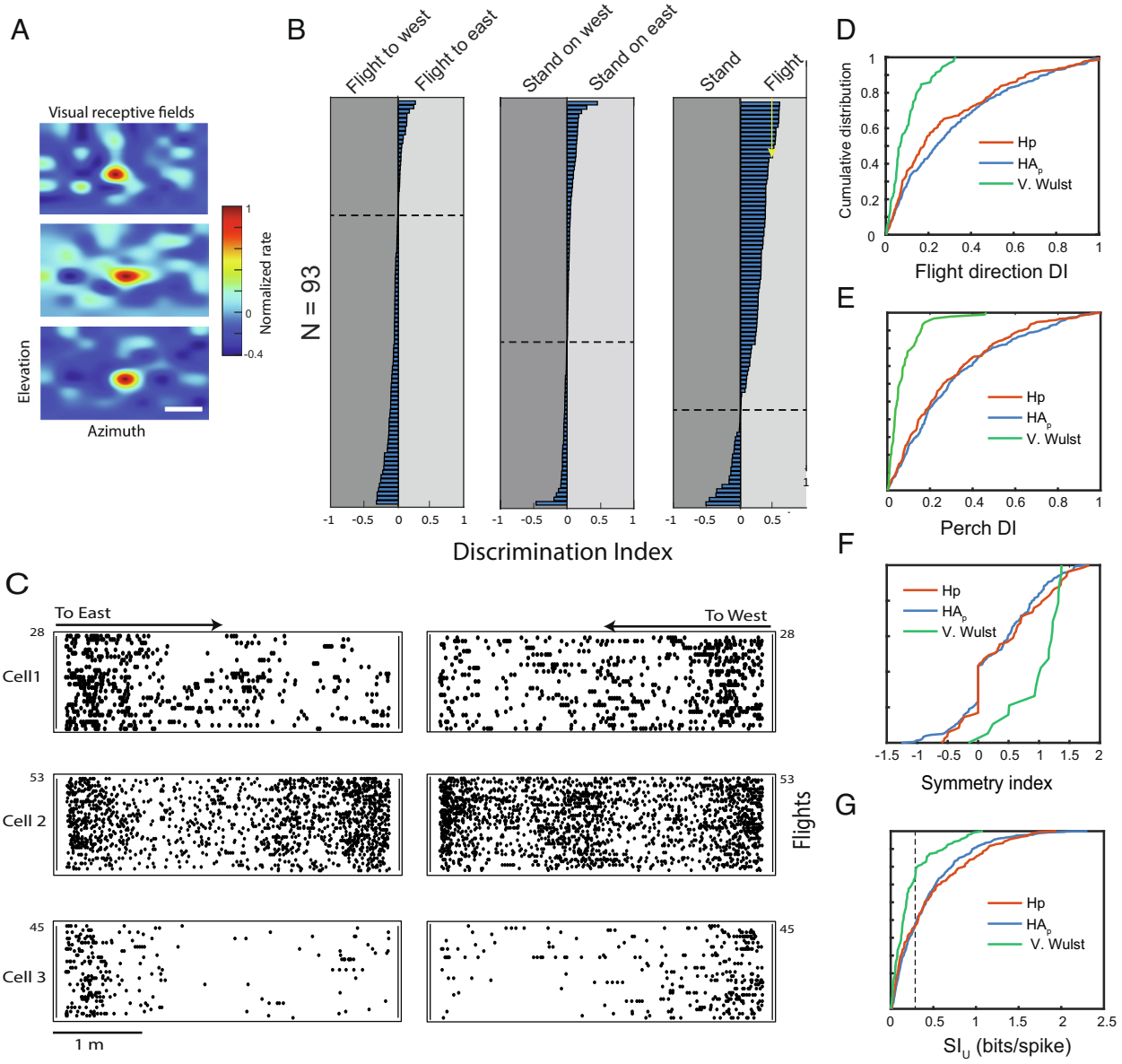

Fig. 6. Recordings from visual Wulst, and comparison between Hp, HA_p, and visual Wulst. (*A*) Visual RF of three neurons recorded in the visual Wulst, in a head fixed experiment. Color plots show the smoothed normalized responses (firing-rates after stimulus onset minus firing-rates before stimulus onset) as a function of the position of the visual stimulus on the screen. (Scale bar, 10°.) (*B*) Summary of the DIs between flight-directions (*Left* plot), perch locations (*Middle* plot), and flight versus standing (*Right* plot), for all the neurons recorded in the visual Wulst (n = 93). Plotted as in Fig. 2*D*. The Y-axis represents the neurons, sorted by the discrimination-index. Vertical arrow in the right plot marks the neurons with values large than 0.5; notably, in the left and middle plots all values were smaller than 0.5. (*C*) Examples of spike-rasters during flights for three cells in the visual Wulst, which passed the criteria for place-cells. *Left* column, spikes during eastbound flights; *Right* column, spikes during westbound flights. Arrows indicate the beginning and direction of flights for each raster. Numbers on the Y-axis designate the number of trials in each raster. (*D*) Cumulative distributions of the DIs between flight directions. Results are from the population of neurons that significantly discriminated between directions in the three brain regions: Hp, HA_p and the visual Wulst. (*E*) Same as in *D* but between perches. (*F*) Cumulative distributions of the symmetry indices from all place-cells in the three brain regions. (*G*) Cumulative distributions of the spatial information indices (SI) from all spatially modulated firing-rate maps, in Hp, HA_p and the visual Wulst. The dashed-line marks the SI value used here as a criterion for place cells (0.3).

could not explore place cells during a volumetric 3D flight that fills 3D space, as was done in flying bats (52). Instead, we chose to explore firing rates during stereotypical perch-to-perch flights. This 1D behavior is comparable to a linear track behavior in mammalian species (53). Multiple studies investigated the firing of place-cells in animals walking back-and-forth along a linear path, and have reported spatial tuning that differs between both running-directions (54–56). Directionality of place tuning was found also during back-and-forth 1D flying in bats (43, 44). Similarly, place cells recorded recently in the titmouse (a food-caching bird) also showed direction-dependent place-fields in a linear track behavior (31). Many of the neurons recorded in the barn owl showed a similar behavior: namely, their firing-rates were significantly modulated by the position along the flight path, and this place-tuning was different for each direction. Spatial and directional modulations were stable during the recording session and were robust to salient changes in the lighting and in the position of the experimenter in the room. Moreover, robust place-coding and directional selectivity were also found in a nonrepetitive flight task in which the owls flew between four perches to obtain a reward, covering larger portions of the room. Therefore, our findings suggest the existence of

place-cells in the hippocampal formation (Hp) and in the posterior part of the hyperpallium apicale (HA_p), but see anatomical discussion below.

In addition to place cells that were spatially tuned during flight, some of the cells robustly discriminated between the perches while the owls were standing in-between flights—perhaps similar to hippocampal CA2 neurons in rats that were reported to encode the rat's position during immobility (57).

Although our findings are consistent with place-cells, one possibility that should be considered is that we are recording from visual neurons that are sensitive to a specific visual cue that passes through a visual receptive-field. In stereotypic flights, a certain cue in the room is expected to appear consistently at a certain location and direction (58). In some studies in rodents and bats, direct visual influence has been ruled out by having the animals walk or fly in complete darkness (43, 59). Unfortunately, this control experiment cannot be performed here because barn owls do not fly between perches in complete darkness. However, other findings do not support this visual-based possibility. First, different cells recorded in the same owl showed opposite direction sensitivities (*SI Appendix*, Table S1). Visual RFs in the hyperpallium of barn owls are organized retinotopically to map the contralateral side (20). Therefore, if these were classical visual neurons, the responses of neurons in a single side of the brain are expected to be directional correlated, i.e., display similar directional tunings. Second, cells recorded in the four-perch feeder experiments, with multiple crossing flight paths, showed high response specificity to spatial location and direction—which does not seem consistent with retinotopically tuned visual responses. Third, switching lighting-direction in the room did not correspondingly switch the directional preference. Fourth and finally, we manually projected an ophthalmoscope light on the owls' eyes and searched for visually evoked responses: clear visual-evoked responses were apparent in the recordings from the visual Wulst, but not in the other recordings. Recordings from the visual Wulst, a well-known primary visual area, showed cells that were significantly modulated by position and direction—but less robustly than in Hp and HA_p. Importantly, place-tuned neurons in the visual Wulst showed highly symmetrical responses (mirror image) between the two flight directions. Symmetrical responses in a linear-track behavior have been related to distance-coding and not place coding (60) and were found in the anterior cingulate cortex (61) and in some hippocampal place-cells in virtual reality (60). The symmetrical spatial modulation in the visual Wulst may reflect sensitivity of the visual neurons to the changes in optic flow during flight, which are expected to be correlated with distances from the incoming walls (62).

Some of the recorded cells exhibited multiple place-fields in the flight tasks (*SI Appendix*, Fig. S10 and examples in *SI Appendix*, Figs. S5, S7 and S8). This observation is consistent with findings of multiple place-fields in hippocampal dorsal CA1 of bats flying in a much longer linear environment (44). It is also consistent with reports on rodent grid cells in linear tracks, which also exhibit multiple fields, often not regularly spaced (63). Future work will need to examine whether these observed responses are more hippocampus-like or more entorhinal-like in terms of the neuronal functional properties.

We found here robust spatial modulation of neurons both in the owl hippocampus (Hp), and in a neighboring region—the posterior part of the hyperpallium apicale (HA_p). The HA, including the HA_p, is the upper layer of the hyperpallium. In one leading theory, the HA is comparable to neocortical layers V-VI (17). The anterior part of the hyperpallium is a somatosensory area (64) and posterior to it is a primary visual area (visual Wulst) (20, 65). However, the function of the most posterior and medial areas of the hyperpallium is unknown (66). Moreover, the functional borders between Hp and HA_p are not clearly defined (67). It is therefore difficult to compare the anatomy of our findings with that of mammals or even with other bird species. Immunohistochemical labeling of various neuronal markers suggest that, in several avian species, the dorsal lateral part of the hippocampal formation is extended further laterally from the edge of the lateral ventricle (14, 68). We therefore cannot rule out the possibility that our recording sites in HA_p are, in fact, part of an extended rostral and lateral Hp. Another possibility is that place-cells in birds are not limited to the hippocampal formation. The most posterior parts of the hyperpallium may be part of a broader pallial network of spatial representation that includes the Hp as well as other pallial regions (14, 66, 68–70). In mammals, place cells have been primarily described as a hippocampal phenomenon; however, place cells have been found also in several other cortical areas (58, 71–73), expanding the cortical network of spatial representation beyond the hippocampal formation.

The study of neural representations in the avian Hp is at its infancy relative to mammals. Yet, the accumulating data, together with the results reported here, already cover five distinct bird species (26, 30, 31). Although it is difficult to compare between the different behavioral tasks used in these studies—flying in straight lines in the current study versus hopping/walking in 2D (26, 31) versus walking in radial mazes (28)—the emerging view is of substantial variability between species. Titmouses with their unique capability to memorize the locations of thousands of seeds have an enlarged hippocampus as well as an exceptional abundance of place-cells (31). Here, in the barn owl—a nonfood caching bird which is a central-place forager that relies on spatial memory to navigate to its roost at night (33)—we found a robust place-cell representation. Future studies across multiple bird species are required to elucidate the extent to which the occurrence of place-cells is correlated with ecological reliance on spatial memory.

Materials and Methods

Animals. Seven adult Barn Owls (*Tyto alba*) were used for the study (four females and two males; Arya, DB, TLV, DB2, DK, Waldo and BB; see *SI Appendix*, Table S1). The owls were hatched in our in-house breeding colony and were hand-raised from 10 to 60 d of age, and thus were well acclimatized to human presence and handling. All procedures were approved by the Technion's Institutional Animal Care and Use Committee and were in accordance with the Israeli law for the prevention of cruelty to animals.

Behavioral Setup. Experiments were conducted in a 4 × 2.2 × 2.4-m windowless room, dimly lit by three nonflickering LED light sources. The short walls of the room faced east and west, and the long walls faced south and north. In the first experiment–the "two-perch experiment"–the room contained two wooden standing-perches (1.7 m above the ground, 50 cm long, 10 cm wide, and parallel to the wall), one on the east wall and one on the opposing west wall (Movie S1). The door to the room was on the south wall adjacent to the east- south corner. Between experiments the owls stayed in the experimental flight room.

At the beginning of the recording session, the owl was released in the room and typically flew to one of the perches to stand there. In this experiment, the owls were not trained with rewards to fly between perches. Instead, the experimenter entered the room and stood adjacent to the south wall (in a few control experiments, the experimenter moved in midsession to the opposite wall). When the owl was standing on one of the perches, the experimenter made a gesture toward the owl, by either stepping slowly toward it or slowly moving the arm on the side of the owl. The owls we used were hand-raised and accustomed to the presence of humans. Yet, they still naturally prefer to maintain distance from a human in the room, which encouraged the owl to fly to the other side in response to the experimenter's gesture. This procedure was repeated every day for ~20 min. The owls quickly adjusted and learned to respond to small experimenter's gestures, by flying to the opposite perch, often flying spontaneously back and forth multiple

times without any movements by the experimenter. During a 20-min session, owls flew on average 82 ± 20 flights (mean ± SD). We note that the owls in this experiment did not show signs of stress, such as head bobbing, unfolding wings when standing, beak clicking, or erratic flights.

In a second experiment—the "four-perch experiment with a feeder"—we mounted four perches 1.7 m above the ground, one on each of the four walls of the room (in the same flight-room used for the first experiment). For this experiment, the owls were trained to obtain food (pieces of chicken meat) from an Arduino-controlled feeder box. The box contained a circular plate with 30 food-holding wells. The plate rotation and the opening of the feeder door were controlled by servo motors. A brief tone and an LED light indicated the opening of the feeder door and the availability of a food reward. Food reward was offered for 20 s after the sound. If reward was not taken within 20 s, the feeder door was closed.

The owls were first adapted to obtain their daily food portion from the feeder in their home cage. When ready, the owls underwent a surgery to implant tetrodes (see details below), and after a few days of recovery began the experiments. The feeder was mounted on one of the perches, and stayed there for the entire daily session; every experimental day the feeder position was changed to a different perch. Out of the three remaining perches, one perch was randomly assigned to be the target-perch. For the feeder to open and offer a reward, the owl had to fly to the target-perch and stand on it for 1 s. From there, the owl had 20 s to fly to the feeder and take the reward. After every opening of the feeder, the target-perch was randomly reselected with equal probability between the three perches. Therefore, every trial the owl had to search for the target perch by flying between perches. A MATLAB code was used to integrate the online 3D motion tracking data (see below) for controlling the experiment in a fully automated manner, without an experimenter in the room throughout the session.

In all behavioral experiments, the 3D position of the owl was tracked in real-time at a rate of 120 Hz, via eight high-speed infrared cameras (OptiTrack) placed around the room. Details of behavioral tracking can be found in the *SI Appendix*.

Surgery and Neural Recordings. Owls were prepared for chronic electrophysiological recordings with a single surgical procedure. Details of surgery can be found in the *SI Appendix*. To determine craniotomy positions, distances on the skull were measured, with a fine surgical caliper, from the anterior edge of the dorsal neck muscle (tendon attachment position on the skull)–which is the standard cranial landmark used in barn owls. Coordinates for the hippocampus (Hp): 13 mm anterior from the muscle and 2 to 3 mm lateral from the midline. For the posterior part of hyperpallium apicale (HA_p): 14 to 15 mm anterior from the muscle and 2.5 to 3.5 mm lateral from the midline. For the visual Wulst: 18 mm anterior and 6 mm lateral from the midline.

We used a custom-made microdrive (74), containing four tetrodes. Neuronal signals were recorded using a 16-channel wireless neural-recording device ("neural logger," Spikelog-16, Deuteron Technologies). Details of recording set-up can be found in the *SI Appendix*. Signals were bandpass filtered on-board (300 to 7,000 Hz), thus analysis of local field potential oscillations is precluded. Recording sessions were performed almost every day, typically for a few weeks, until signal-to-noise ratio dropped. Tetrodes were advanced by 50 μm every day. If no spikes were detected, tetrodes were continuously lowered until spikes were observed, until reaching a depth of about 1,500 μm below the brain surface. In some of the owls, the microdrive was carefully removed at the end of the experiment and a new microdrive was installed several months later, in the opposite hemisphere, for further recordings (*SI Appendix*).

Histology and Micro-CT. To enable repeated measurements in different brain regions, most of the owls in this experiment were not euthanized for histology. Instead, we used the stereotaxic coordinates to tell apart recording locations in Hp versus HA_p (the recording locations in the visual Wulst were verified based on visual neuronal responses: Fig. 6*A*). Because we did not euthanize and did not histologically analyze most of the owls at the end of the experiments, we cannot rule out the possibility that the anatomical position of some of the recorded neurons in our Hp recordings were slightly lateral to the lateral edge or vice versa. However, use of stereotaxic coordinates should provide a good separation of recording sites to Hp versus HA_p–because i) Hp and hyperpallium are large in barn owls, ii) there were relatively large distances of a few millimeters between the coordinate sets used to target Hp and HA_p (see coordinates above), and iii) because the recordings are superficial in the brain. We are thus confident that the bulk of the population is anatomically segregated, as expected from the very-distinct stereotaxic coordinates. In two owls, we performed standard histology, and in two other owls we performed micro CT scans to verify recording locations. Details of histology and CT protocols can be found in the *SI Appendix*.

Data Processing and Spike Sorting. In subsequent processing (offline), electrical recordings were band-pass filtered between 600 and 6,000 Hz, and manual spike sorting was performed using the SpikeSort3D software (Neuralynx). Details about data processing and spike sorting can be found in the *SI Appendix*. A spike was included for further analysis if its shape matched with any of the spike templates from a preexisting database (template matching: Pearson-correlation coefficient >0.8), if its 3D cluster was above noise level (not truncated) and a refractory period (<2 ms) was apparent in the interspike-interval histogram. Single units with less than 50 spikes in a session were excluded. To assess the quality of single-unit spike sorting (clustering), we used the isolation distance and L-ratio, two standard measures of spike-sorting quality (75). The median isolation distance and L-ratio were 18 and 0.18, respectively, indicating reasonably good quality of spike sorting (75). Importantly, the percentage of place-cells in the recorded population remained similar when considering only cells with higher clustering quality versus when considering all isolated clusters (*SI Appendix*, Table S3).

Data Analysis. Analyses of all the behavioral and neural data were done using custom Matlab codes. Details of the analysis can be found in the *SI Appendix*.

Data, Materials, and Software Availability. The dataset of the spike trains of the single units generated in this study, the behavioral tracking data and additional results of the analysis are available at Mendeley Data: DOI: 10.17632/2dj4z7x2tx.1 (76).

ACKNOWLEDGMENTS. We thank Tidhar Lev-Ari, Hadar Beeri, Liora Las, and Shaked Ron for assistance and advice. This work was supported by research grants from the Rappaport Institute for Biomedical Research, the Adelis Foundation, and the Israel Science Foundation (grant no. 2655/18 to Y.G., D.D. and N.U.). Y.G. also acknowledges the generous support of the Edward S. Mueller Eye Research Fund and the Irving and Branna Sisenwine Fund.

1. J. O'Keefe, J. Dostrovsky, The hippocampus as a spatial map. Preliminary evidence from unit activity in the freely-moving rat. *Brain. Res.* **34**, 171–175 (1971).
2. J. S. Taube, R. U. Muller, J. B. Ranck, Head-direction cells recorded from the postsubiculum in freely moving rats. I. Description and quantitative analysis. *J. Neurosci.* **10**, 420–435 (1990).
3. T. Hafting, M. Fyhn, S. Molden, M. B. Moser, E. I. Moser, Microstructure of a spatial map in the entorhinal cortex. *Nature* **436**, 801–806 (2005).
4. M. M. Yartsev, M. P. Witter, N. Ulanovsky, Grid cells without theta oscillations in the entorhinal cortex of bats. *Nature* **479**, 103–107 (2011).
5. A. Finkelstein *et al.*, Three-dimensional head-direction coding in the bat brain. *Nature* **517**, 159–164 (2015).
6. J. O'Keefe, L. Nadel, *The Hippocampus as a Cognitive Map* (Clarendon Press; Oxford University Press, Oxford, New York, 1978), **vol. 14**, p. 570.
7. H. Eichenbaum, The role of the hippocampus in navigation is memory. *J. Neurophysiol.* **117**, 1785–1796 (2017).
8. M. B. Moser, D. C. Rowland, E. I. Moser, Place cells, grid cells, and memory. *Cold. Spring. Harb. Perspect. Biol.* **7**, a021808 (2015).
9. C. Herold, V. J. Coppola, V. P. Bingman, The maturation of research into the avian hippocampal formation: Recent discoveries from one of the nature's foremost navigators. *Hippocampus* **25**, 1193–1211 (2015).
10. A. Reiner, K. Yamamoto, H. J. Karten, Organization and evolution of the avian forebrain. *Anat. Rec. A. Discov. Mol. Cell Evol. Biol.* **287**, 1080–1102 (2005).
11. Y. Atoji, J. M. Wild, Anatomy of the avian hippocampal formation. *Rev. Neurosci.* **17**, 3–15 (2006).
12. C. C. Chen, C. M. Winkler, A. R. Pfenning, E. D. Jarvis, Molecular profiling of the developing avian telencephalon: Regional timing and brain subdivision continuities. *J. Comp. Neurol.* **521**, 3666–3701 (2013).
13. M. Colombo, N. Broadbent, Is the avian hippocampus a functional homologue of the mammalian hippocampus? *Neurosci. Biobehav. Rev.* **24**, 465–484 (2000).
14. A. D. Székely, The avian hippocampal formation: Subdivisions and connectivity. *Behav. Brain Res.* **98**, 219–225 (1999).
15. L. Medina, A. Abellán, "Development and evolution of the pallium" in *Seminars in Cell & Developmental Biology* (Elsevier, 2009), pp. 698–711.
16. H. J. Karten, Vertebrate brains and evolutionary connectomics: On the origins of the mammalian "neocortex". *Philos. Trans. R. Soc. Lond. B Biol. Sci.* **370**, 20150060 (2015).
17. M. Stacho *et al.*, A cortex-like canonical circuit in the avian forebrain. *Science* **369**, eabc5534 (2020).
18. Y. Atoji, J. M. Wild, Fiber connections of the hippocampal formation and septum and subdivisions of the hippocampal formation in the pigeon as revealed by tract tracing and kainic acid lesions. *J. Comp. Neurol.* **475**, 426–461 (2004).

19. A. Reiner *et al.*, Revised nomenclature for avian telencephalon and some related brainstem nuclei. *J. Comp. Neurol.* **473**, 377–414 (2004).
20. J. D. Pettigrew, Binocular visual processing in the owl's telencephalon. *Proc. R. Soc. Lond. B Biol. Sci.* **204**, 435–454 (1979).
21. S. Watanabe, H. J. Bischof, Effects of hippocampal lesions on acquisition and retention of spatial learning in zebra finches. *Behav. Brain. Res.* **155**, 147–152 (2004).
22. T. V. Smulders, T. J. DeVoogd, Expression of immediate early genes in the hippocampal formation of the black-capped chickadee (Poecile atricapillus) during a food-hoarding task. *Behav. Brain. Res.* **114**, 39–49 (2000).
23. A. Gagliardo, P. Ioale, V. P. Bingman, Homing in pigeons: The role of the hippocampal formation in the representation of landmarks used for navigation. *J. Neurosci.* **19**, 311–315 (1999).
24. D. F. Sherry, S. L. Grella, M. F. Guigueno, D. J. White, D. F. Marrone, Are there place cells in the avian hippocampus? *Brain Behav. Evol.* **90**, 73–80 (2017).
25. S. Watanabe, U. Mayer, H. J. Bischof, Visual Wulst analyses "where" and entopallium analyses "what" in the zebra finch visual system. *Behav. Brain Res.* **222**, 51–56 (2011).
26. E. Ben-Yishay *et al.*, Directional tuning in the hippocampal formation of birds. *Curr. Biol.* **31**, 2592–2602.e2594 (2021).
27. V. P. Bingman, G. E. Hough 2nd, M. C. Kahn, J. J. Siegel, The homing pigeon hippocampus and space: In search of adaptive specialization. *Brain. Behav. Evol.* **62**, 117–127 (2003).
28. G. E. Hough, V. P. Bingman, Spatial response properties of homing pigeon hippocampal neurons: Correlations with goal locations, movement between goals, and environmental context in a radial-arm arena. *J. Comp. Physiol. A Neuroethol. Sens. Neural. Behav. Physiol.* **190**, 1047–1062 (2004).
29. M. C. Kahn, V. P. Bingman, Lateralization of spatial learning in the avian hippocampal formation. *Behav. Neurosci.* **118**, 333–344 (2004).
30. M. C. Kahn, J. J. Siegel, T. J. Jechura, V. P. Bingman, Response properties of avian hippocampal formation cells in an environment with unstable goal locations. *Behav. Brain Res.* **191**, 153–163 (2008).
31. H. Payne, G. Lynch, D. Aronov, Neural representations of space in the hippocampus of a food-caching bird. *Science* **373**, 343–348 (2021).
32. R. S. Payne, Acoustic location of prey by barn owls (Tyto alba). *J. Exp. Biol.* **54**, 535–573 (1971).
33. G. Rozman, I. Izhaki, A. Roulin, M. Charter, Movement ecology, breeding, diet, and roosting behavior of barn owls (Tyto alba) in a transboundary conflict region. *Reg. Environ. Change* **21**, 1–13 (2021).
34. M. Konishi, Study of sound localization by owls and its relevance to humans. *Comp. Biochem. Physiol. A Mol. Integr. Physiol.* **126**, 459–469 (2000).
35. J. L. Pena, Y. Gutfreund, New perspectives on the owl's map of auditory space. *Curr. Opin. Neurobiol.* **24**, 55–62 (2014).
36. J. D. Pettigrew, M. Konishi, Neurons selective for orientation and binocular disparity in the visual Wulst of the barn owl (Tyto alba). *Science.* **193**, 675–678 (1976).
37. F. Lormant *et al.*, Research note: Role of the hippocampus in spatial memory in Japanese quail. *Poultry Sci.* **99**, 61–66 (2020).
38. K. Mizuseki, A. Sirota, E. Pastalkova, G. Buzsáki, Theta oscillations provide temporal windows for local circuit computation in the entorhinal-hippocampal loop. *Neuron* **64**, 267–280 (2009).
39. H. J. Karten, W. Hodos, *A Stereotaxic Atlas of the Pigeon Brain* (The Johns Hopkins Press, Baltimore, Maryland, 1967).
40. S. Edut, D. Eilam, Protean behavior under barn-owl attack: Voles alternate between freezing and fleeing and spiny mice flee in alternating patterns. *Behav. Brain. Res.* **155**, 207–216 (2004).
41. J. Baylé, Stereotaxic topography of the brain of the quail. *J. Physiol. Paris* **68**, 219–241 (1974).
42. S. A. Hollup, S. Molden, J. G. Donnett, M. B. Moser, E. I. Moser, Accumulation of hippocampal place fields at the goal location in an annular watermaze task. *J. Neurosci.* **21**, 1635–1644 (2001).
43. M. Geva-Sagiv, S. Romani, L. Las, N. Ulanovsky, Hippocampal global remapping for different sensory modalities in flying bats. *Nat. Neurosci.* **19**, 952–958 (2016).
44. T. Eliav *et al.*, Multiscale representation of very large environments in the hippocampus of flying bats. *Science* **372**, eabg4020 (2021).
45. A. Nieder, H. Wagner, Perception and neuronal coding of subjective contours in the owl. *Nat. Neurosci.* **2**, 660–663 (1999).
46. A. Nieder, H. Wagner, Horizontal-disparity tuning of neurons in the visual forebrain of the behaving barn owl. *J. Neurophysiol.* **83**, 2967–2979 (2000).
47. J. Baron, L. Pinto, M. O. Dias, B. Lima, S. Neuenschwander, Directional responses of visual wulst neurones to grating and plaid patterns in the awake owl. *Eur. J. Neurosci.* **26**, 1950–1968 (2007).
48. W. E. Skaggs, B. L. McNaughton, M. A. Wilson, C. A. Barnes, Theta phase precession in hippocampal neuronal populations and the compression of temporal sequences. *Hippocampus* **6**, 149–172 (1996).
49. A. A. Fenton, R. U. Muller, Place cell discharge is extremely variable during individual passes of the rat through the firing field. *Proc. Natl. Acad. Sci. U.S.A.* **95**, 3182–3187 (1998).
50. J. Jackson, A. D. Redish, Network dynamics of hippocampal cell-assemblies resemble multiple spatial maps within single tasks. *Hippocampus* **17**, 1209–1229 (2007).
51. A. Roulin, *Barn Owls: Evolution and Ecology* (Cambridge University Press, 2020).
52. M. M. Yartsev, N. Ulanovsky, Representation of three-dimensional space in the hippocampus of flying bats. *Science* **340**, 367–372 (2013).
53. L. Las, N. Ulanovsky, "Hippocampal neurophysiology across species" in *Space, Time and Memory in the Hippocampal Formation* (Springer, 2014), pp. 431–461.
54. J. O'Keefe, M. L. Recce, Phase relationship between hippocampal place units and the EEG theta rhythm. *Hippocampus* **3**, 317–330 (1993).
55. B. L. McNaughton, C. A. Barnes, J. O'Keefe, The contributions of position, direction, and velocity to single unit activity in the hippocampus of freely-moving rats. *Exp. Brain. Res.* **52**, 41–49 (1983).
56. Y. Ziv *et al.*, Long-term dynamics of CA1 hippocampal place codes. *Nat. Neurosci.* **16**, 264–266 (2013).
57. K. Kay *et al.*, A hippocampal network for spatial coding during immobility and sleep. *Nature* **531**, 185–190 (2016).
58. A. B. Saleem, E. M. Diamanti, J. Fournier, K. D. Harris, M. Carandini, Coherent encoding of subjective spatial position in visual cortex and hippocampus. *Nature* **562**, 124–127 (2018).
59. S. Zhang, F. Schönfeld, L. Wiskott, D. Manahan-Vaughan, Spatial representations of place cells in darkness are supported by path integration and border information. *Front. Behav. Neurosci.* **8**, 222 (2014).
60. P. Ravassard *et al.*, Multisensory control of hippocampal spatiotemporal selectivity. *Science* **340**, 1342–1346 (2013).
61. A. Rubin *et al.*, Revealing neural correlates of behavior without behavioral measurements. *Nat. Commun.* **10**, 4745 (2019).
62. J. R. Serres, F. Ruffier, Optic flow-based collision-free strategies: From insects to robots. *Arthropod. Struct. Dev.* **46**, 703–717 (2017).
63. D. Derdikman *et al.*, Fragmentation of grid cell maps in a multicompartment environment. *Nat. Neurosci.* **12**, 1325–1332 (2009).
64. J. M. Wild, The avian somatosensory system: The pathway from wing to Wulst in a passerine (Chloris chloris). *Brain Res.* **759**, 122–134 (1997).
65. H. J. Karten, W. Hodos, W. J. Nauta, A. M. Revzin, Neural connections of the "visual wulst" of the avian telencephalon. Experimental studies in the piegon (Columba livia) and owl (Speotyto cunicularia). *J. Comp. Neurol.* **150**, 253–278 (1973).
66. H. J. Karten, W. Hodos, W. J. Nauta, A. M. Revzin, Neural connections of the "visual wulst" of the avian telencephalon. Experimental studies in the piegon (Columba livia) and owl (Speotyto cunicularia). *J. Comp. Neurol.* **150**, 253–278 (1973).
67. C. Herold *et al.*, The hippocampus of birds in a view of evolutionary connectomics. *Cortex* **118**, 165–187 (2019).
68. D. Heyers *et al.*, Morphology, biochemistry and connectivity of Cluster N and the hippocampal formation in a migratory bird. *Brain. Struct. Funct.* **17**, 022–02566 (2022).
69. J. T. Erichsen, V. P. Bingman, J. R. Krebs, The distribution of neuropeptides in the dorsomedial telencephalon of the pigeon (Columba livia): A basis for regional subdivisions. *J. Comp. Neurol.* **314**, 478–492 (1991).
70. G. Casini, V. P. Bingman, P. Bagnoli, Connections of the pigeon dorsomedial forebrain studied with WGA-HRP and 3H-proline. *J. Comp. Neurol.* **245**, 454–470 (1986).
71. E. M. Diamanti *et al.*, Spatial modulation of visual responses arises in cortex with active navigation. *Elife* **10**, e63705 (2021).
72. X. Long, S.-J. Zhang, A novel somatosensory spatial navigation system outside the hippocampal formation. *Cell Res.* **31**, 649–663 (2021).
73. I. M. Esteves *et al.*, Spatial information encoding across multiple neocortical regions depends on an intact hippocampus. *J. Neurosci.* **41**, 307–319 (2021).
74. S. Weiss *et al.*, Consistency of spatial representations in rat entorhinal cortex predicts performance in a reorientation task. *Curr. Biol.* **27**, 3658–3665.e3654 (2017).
75. N. Schmitzer-Torbert, J. Jackson, D. Henze, K. Harris, A. Redish, Quantitative measures of cluster quality for use in extracellular recordings. *Neuroscience* **131**, 1–11 (2005).
76. A. Agarwal, A. Sarel, D. Derdikman, N. Ulanovsky, Y. Gutfreund, Spatial coding in the hippocampus and hyperpallium of *flying* owls. Mendeley Data. https://data.mendeley.com/datasets/2dj4z7x2tx/1. Deposited 21 December 2022.

PNAS

Supporting Information for
Spatial coding in the hippocampus and hyperpallium of flying owls.

Arpit Agarwal, Ayelet Sarel, Dori Derdikman, Nachum Ulanovsky, and Yoram Gutfreund

Corresponding author: Yoram Gutfreund
Email: yoramg@technion.ac.il

This PDF file includes:

Other supporting materials for this manuscript include the following:

Movies S1 to S3 in separate files.

Supporting Information Text

Extended Methods

Surgery: the birds were anaesthetized with 2% isoflurane in a 4:5 mixture of nitrous oxide and oxygen. Owls were then positioned in a stereotaxic frame (Kopf, small animals instrument Model 963) using custom-made ear bars. Lidocaine (Lidocaine HCl 2% and Epinephrine) was injected locally at the incision site. The skull was exposed and cleaned. Four skull screws were inserted at the posterior part of the skull and one ground screw was inserted at the right frontal part of the skull. A 2-mm diameter craniotomy was drilled around the desired position and a small nick in the dura was made at the center of the craniotomy using a surgical needle. The microdrive was carefully lowered until the tetrodes smoothly entered the brain tissue. Penetration was stopped 400 µm below the brain surface. Antibiotic ointment (Chloramfenicol 5%) was applied to the brain surface, followed by a thin coat of a silicon elastomer (Kwik-Sil). The microdrive was then connected to the ground screw with a silver wire and attached to the skull with adhesive cement (C&B Metabond) and light-cured dental resin (Spident Inc. EsFlow). The exposed skull is covered with a layer of dental cement and the skin edges with VetBond. The owls were then positioned in a heated chamber to recover.

Recording: We used a custom-made microdrive, modified from the microdrive described in Weiss *et al.*, Consistency of spatial representations in rat entorhinal cortex predicts performance in a reorientation task. *Current Biology* **27**, 3658-3665. e3654 (2017). The microdrive holds four tetrodes made of 17.8 µm platinum-iridium wire (California Fine Wire); the tetrodes were platinum-black plated to reduce the impedance to 500–800 kOhm at 1 kHz. Neuronal signals were recorded using a 16-channel wireless neural-recording device ('neural logger', Spikelog-16, Deuteron Technologies) which was attached to the Omnetics connector on the microdrive. Signals from all 16 channels of the 4 tetrodes were amplified (×200), bandpass filtered (300 – 7,000 Hz) and sampled continuously at 29.3 kHz per channel. Data were stored on-board the neural-logger. Recording sessions were performed almost every day, typically for a few weeks, until signal-to-noise ratio dropped. Tetrodes were advanced by 50 µm every day. If no spikes were detected, tetrodes were continuously lowered until spikes were observed. After reaching a depth of 1,500 µm below the brain surface, in some of the experiments the tetrodes were retracted to regions of previously-observed spiking activity, and additional experiments were conducted. At the end of the experiment the microdrive and tetrodes were carefully removed, the craniotomy was sealed using Kwik-Sil and dental cement. In some of the

owls a new microdrive was installed several months later, in the opposite hemisphere, for further recordings.

Behavioral tracking: The position of the owl in the room was continuously tracked at a rate of 120 Hz, via eight high-speed infrared cameras (OptiTrack, Oregon, USA) placed around the room, which captured the positions of infrared reflectors rigidly attached to the microdrive on the head of the owl. Online 3D reconstruction of the 3D position of the reflectors (accuracy of ~5mm) was achieved with the Motive software (OptiTrack, Oregon, USA). The room coordinates and the 3D position of the perches were also recorded, alongside with the owl's position, by placing infrared markers on the edges of the perches, as well as markers on the floor corner to mark the zero coordinate.

For synchronization between behavioral tracking and neural recordings, we generated random trains of TTL pulses with a mean interval of 2 seconds and a random jitter of ± 50 ms. The timing of these TTL pulses was transmitted wirelessly to the neural-logger and in parallel was transmitted to the computer running the Motive program, and was timestamped and saved on both systems. This allowed precise synchronization of the video data and neural recordings with an accuracy of < 1 ms.

Spike sorting: In subsequent processing (off-line), electrical recordings were band-pass filtered between 600–6,000 Hz The first and last minutes of recordings were discarded to avoid filtering edge effects. Large amplitude artifacts were detected and removed from all channels based on absolute voltage larger than 0.8 mV. Then an adaptive voltage threshold (thr) was used for spike detection:

$$\text{thr} = 4 * median\left(\frac{|x|}{0.6745}\right) \qquad (1)$$

Where x is the filtered recorded signal over a running window of 1 minute, the division by 0.6745 accounts for the relationship between the median of the noise and the standard deviation of a normal distribution. Whenever one channel in a tetrode crossed the threshold value, a 1-ms segment was saved from all channels on the tetrode. . Manual spike sorting was performed using the SpikeSort3D software (Neuralynx) and consisted of plotting the spikes in 3D parameter space, finding the features which gave the best cluster separation – primarily spike amplitudes – and manually selecting well-isolated clusters. Coincidence-detection algorithm was used to further identify and remove noise, where equal-amplitude events occurring simultaneously between different tetrodes were removed from analysis. Additionally, all detected spikes were compared to a pre-existing spike-shape database (template matching) by correlating different segments of the spike shape to each template from the

database: A spike was included for further analysis if its Pearson-correlation coefficient with any of the spike templates was larger than 0.8. Spikes were categorized as multi-unit or single-unit, taking into account their clusters, spike shapes, and a refractory period (<2 ms) in the interspike-interval histogram. Spikes considered multi-units were not analyzed.

Histology: In 2 owls we performed histology. Electrical lesions were performed by injecting a positive current through one of the tetrodes (+5 μA for 20 sec). A week later, the owl was deeply anesthetized and perfused with phosphate buffer saline (PBS) solution, followed by 4% paraformaldehyde. The brain was removed and stored in 4% paraformaldehyde for 2–3 days at 4□C, then transferred to PBS. Following fixation, the owl's brains were dehydrated in 70%, 80%, 95% and 100% ethanol, cleared in Xylene and embedded in paraffin wax. The paraffin-embedded brains were sectioned in the coronal plane at 5 μm using a microtome (Leica RM 2265). Sections were collected at 40 □m intervals, mounted on super-frost glass slides and dried in an oven at 37□C for 24 hours. After drying the sections, they were deparaffinized in xylene, rehydrated in a diluted ethanol series, and stained with 0.1% Cresyl violet solution (Nissl stain). The sections were then dehydrated, cleared and cover-slipped with DPX mounting medium (Merck).

CT analysis: In two owl, we reconstructed the tetrodes' position in the brain using a micro CT scan. The owl was anesthetized with Ketamine/Xylazine, positioned in a microCT scanner (Bruker) and scanned for six minutes at a resolution of 84 μm. The CT 3D image was registered with an MRI 3D image of a barn owl's brain (ImageJ; Fijiyama plugin) in order to evaluate the position of the tetrodes relative to the lateral ventricle (Fig. S2).

Data analysis: To classify the behavior to perching versus flying, the 3D head trajectory was smoothed (spline smoothing) and the tangential velocity was calculated. A tangential velocity higher than 80 cm/s was classified as flight. In addition, short epochs of velocity lower than 80 cm/s during flight (in U-turns or during short hovering before landing) were included as flights if they happened further than 10 cm from the perch. Epochs of velocity higher than 80 cm/s recorded at a distance of less than 10 cm from the perch were discarded from the analysis. These criteria imply that flight take-off and landing were not analyzed. Flight direction was classified to westbound or eastbound, based on the *x*-direction of the flight velocity (where *x* is the 4-meter long axis of the room, which connected the two perches).

The owl's behavior was mostly restricted to flying between two perches in a nearly straight line (Fig. 1B). Therefore, analyses and statistical tests in this study were reduced to 1D along the horizontal direction. Rare cases where owls landed on the ground or other positions in the room were excluded from analysis. To compute the firing-rate curves (1D firing-rate maps), we used a fixed spatial bin width of 10 cm. The number of spikes in each bin was smoothed with a 1D Gaussian kernel (σ = 1.5 bins). The time spent in each bin was similarly smoothed (occupancy map). The 1D firing-rate map was then obtained by dividing the number of spikes per bin by the occupancy. Firing-rate maps were calculated separately for each flight direction. For producing 2D maps, spike-counts maps and occupancy maps were measured in 10×10 cm bins, 2D-smoothed with a fixed Gaussian kernel (σ = 1.5 bins), and then divided bin-by-bin to obtain the 2D firing rate map.

To quantify the firing-rate differences between the two flight directions we calculated a discrimination index (DI):

$$\text{Discrimination Index} = \frac{fr_1 - fr_2}{fr_1 + fr_2} \qquad (2)$$

where fr_1 is the average firing rate across all flights in one direction and fr_2 is the same for the opposite direction. Cells that fired less than 20 spikes during flight were not included in this analysis. This index varies from –1 (firing only in one direction) to +1 (firing only in the other direction), with 0 indicating no directional discrimination. To assess the statistical significance of the discrimination index we used bootstrap statistics, as follows. The average firing rates of all individual flights in the session were intermixed and bootstrapped to produce a distribution of 1,000 discrimination indices. A result was considered significant if the real discrimination index was larger than 99% of the drawn indices ($p<0.01$).

To quantify the differences between the two perches or between flights versus perching, discrimination indices were calculated as described above. A similar bootstrap analysis was performed to assess significance of the discrimination indices. A value larger than 99% of the bootstrapped indices was considered significant.

Some of the owls showed a consistent behavioral preference to stand on one of the perches more than the other (Fig. S3F). Therefore, for perch discrimination analysis we equalized the time window for spike counts on both perches. If the owl stayed, for example, on the east perch for 15 seconds, then flew to the west perch and stayed there for 2 seconds, we used in both perches a time window of 2

seconds, starting after landing, to measure firing rates. This was repeated for all pairs of standing epochs (each east-perch standing epoch was paired with the subsequent west-perch standing epoch), taking the shorter time in each pair as the window for spike-counts in every pair.

To quantify the spatial modulation (place-tuning) of the firing rates along the flight, the 1D spatial tuning curve (1D firing-rate map) in-flight was smoothed with a 1D Gaussian kernel (σ = 1.5 bins, using 10-cm bins). The smoothed curve was then used to quantify the spatial-information index in bits/spike (Skaggs et al., 1996):

$$SI = \sum_i \left(p_i \frac{\lambda_i \, log_2\left(\frac{\lambda_i}{\lambda}\right)}{\lambda} \right) \qquad (3)$$

Where, λ_i is the firing rate in the i_{th} bin, λ is the overall average firing rate, and P_i is the average occupancy probability per bin. For cells to be included in this analysis we required at least 20 spikes during flight in that direction.

To estimate place-fields size and the number of place-fields (Fig. S10), we first extracted peaks in the smoothed 1D rate maps that were larger than 1.2 standard deviations of the firing-rate map. Then we removed local peaks by disregarding peaks with a dip smaller than 50% of the firing rate of the larger peak. The borders of the field were defined as the area covering 20 % of the main peak firing rate (example in Fig. S10A).

To assess the significance of place-tuning during flight, we generated shuffled data sets, separately for the two flight-directions. Each spike train of each flight in a particular direction was randomly circularly shifted within the flight duration, thus generating a new set of spikes where the spike-train was maintained but the relation between spiking and position was broken; we then computed the firing-rate map and SI for each such shuffle. We repeated this shuffling 1,000 times, and thus 1,000 shuffled spatial-information indices were generated for each neuron. Cells for which the real SI exceeded the 99'th percentile of the corresponding shuffled distribution, in at least one of the directions, were considered as exhibiting significant place-tuning ($p<0.01$). To eliminate inclusion of cells with low spatial information but which were nevertheless significantly modulated due to a high firing rate, we imposed an additional criterion: SI > 0.3 bits/spike in at least one flight direction was required for a significant placed-tuned cell to be considered a place-cell.

To quantify the symmetry of the tuning curves between the two opposite directions we calculated a symmetry index (SymmI) as follows:

$$SymmI = r_{flipped} - r_{nonflipped} \qquad (4)$$

Where $r_{flipped}$ is the Pearson correlation coefficient between the firing-rate map in one direction and the corresponding firing-rate map in the other direction, but flipped in the east-west direction. $r_{non\text{-}flipped}$ is the Pearson correlation coefficient between the rate maps in the two directions, not flipped. If the pattern of the rate map displays a mirror-image, $r_{flipped}$ will be close to +1 and $r_{non\text{-}flipped}$ will be closed to –1. Thus, this index varies between –2 to +2. Large positive values indicate symmetry (mirror image), whereas large negative values indicate cells which code a similar place in both directions.

In the four-perch feeder experiment, we quantified place-tuning by computing SI; the SI was computed using the 2D firing-rate map rather than the 1D firing-rate map as in the first experiment. Only flight data were used to calculate SI. The room was binned to 10x10 cm bins (excluding the perches and 5 cm away from the perches). The time spent in each bin was smoothed (2D Gaussian kernel; σ = 1.5 bins) to create the occupancy map. The number of spikes in each bin were also smoothed (2D Gaussian kernel; σ = 1.5 bins) and divided by the occupancy map to obtain the mean firing-rate per bin (λ_i). Bins in which the owl was less than 100 ms were removed. The probability per bin (P_i) was calculated by dividing the time in the bin by the total flight time. λ_i and P_i were used in equation 3 to calculate the SI.

To address the significance of the SI results in the four-perch feeder experiment, we generated the distribution of the SI for shuffled data. Spike trains were shuffled by decorrelating them from the behavior, by circularly shifting the spike train across the flight time. Shifts were randomly selected with equal probability between 10 sec to total time of flight minus 10 seconds. We then computed the SI for each such shuffle. We repeated this shuffling 1,000 times. Cells for which the real SI exceeded the 99'th percentile of the corresponding shuffled distribution were considered as exhibiting significant place-tuning ($p<0.01$). As in the two-perch experiment, we imposed an additional criterion: SI > 0.5 bits/spike was required for a significant placed-tuned cell to be considered a place-cell. We set here the threshold to 0.5 bits/spike (rather than 0.3 bits/spike as in the previous experiment) because SI values of the 2D firing-rate maps tended to be larger compared to SI values in the 1D firing-rate maps used when the owls flew back and forth between 2 perches. For raster plots, spike data in 2D was transformed to 1D by calculating the projections of data points onto the straight line connecting the

centers of the take-off perch and the landing perch. For display purposes (Figure 5A and C and figure S6) 2D firing-rate maps were further resampled (bin size of 1x1 cm) and interpolated (bicubic interpolation).

To analyze spike rate variability across flights (overdispersion) we computed for each flight *i* the Z-score of the spike counts relative to the mean and standard deviation of the spike counts in the same direction:

$$Z_i = \frac{n_i - mean(n_i)}{std(n_i)} \qquad (5)$$

Where n_i is the number of spikes in a given flight. Flight speeds were extremely constant across flights (Fig. S3), therefore we did not correct for velocity variability. The Z scores from a given cell were compared with a normal distribution (Kolmogorov-Smirnov normality test). Cells with P values smaller than 0.05 were considered overdispersed.

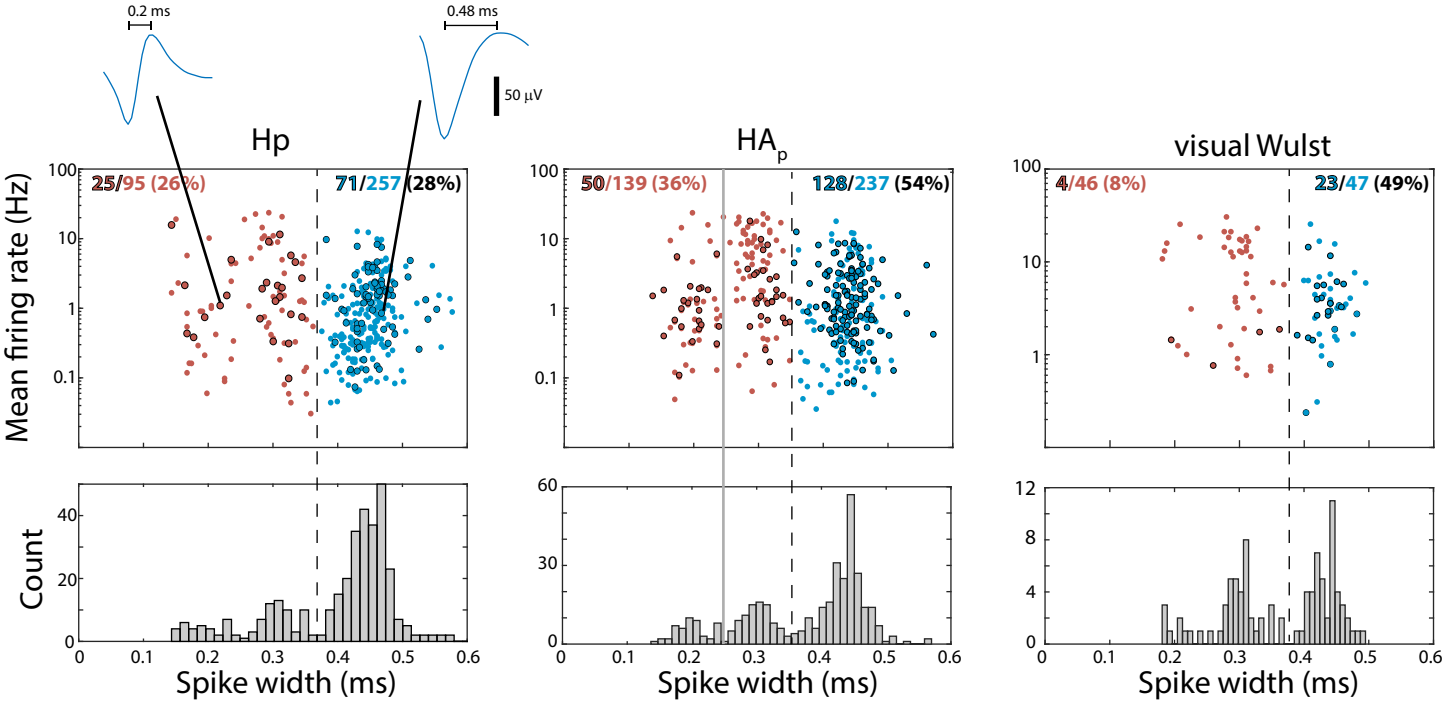

Figure S1. Spike shapes analysis. The mean spike width of all single units used in this study are plotted versus the mean firing rate of the cells. Cells from Hp are shown on the left, cells from HA$_p$ in the middle, and cells from the visual Wulst on the right. Cells were found to cluster into two main groups based on the local minimum of the spike-width histograms (dashed vertical lines). In HA$_p$ the short spikes can be further clustered into two groups (gray line). Dots encircled by a black border designate significant place-cells. Place cells can be found in all three groups. The number of place cells , the number of cells and the percentage of place cells in the two main groups are indicated in the two corresponding corners of each plot. Average shapes of two representative spikes are shown above the left graph.

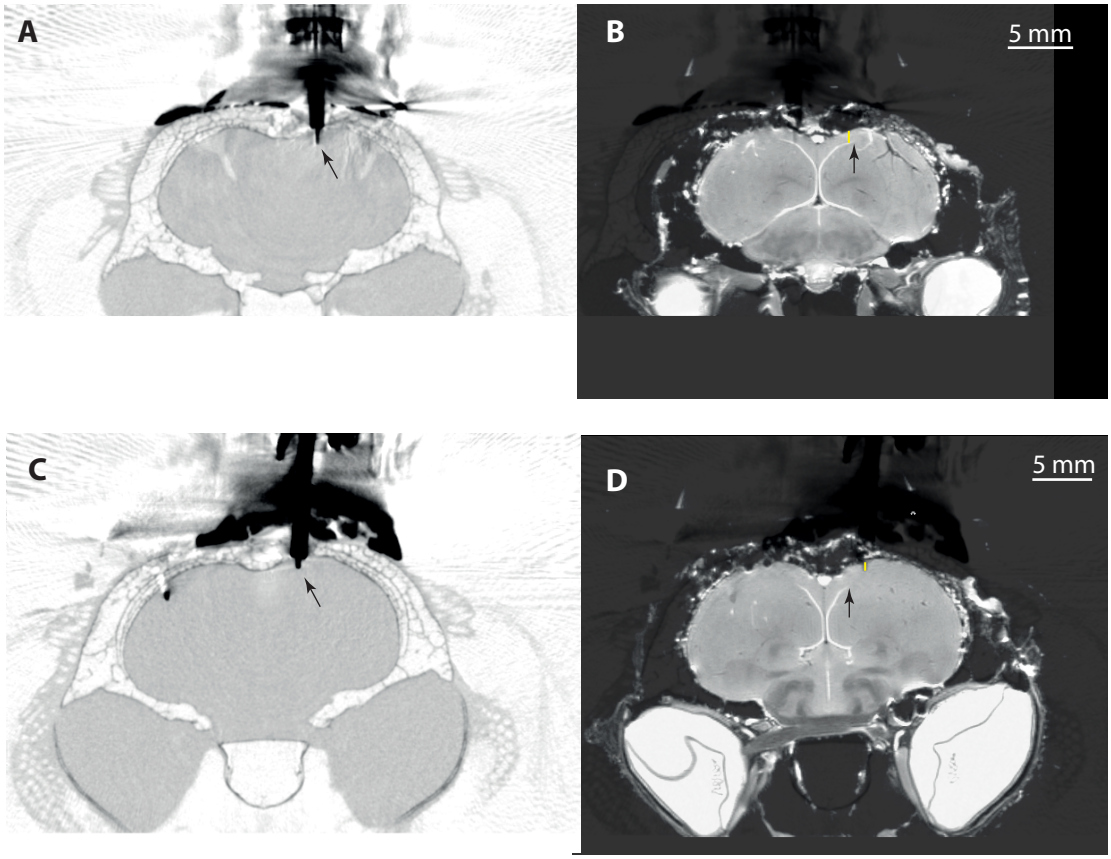

Figure S2. CT based tetrode-track estimation in the Hp and in the HAp of two owls. **A.** Cross section from a full brain CT scan of an owl implanted with tetrodes in the right Hp (owl BB, see Table S1). The image shows a cross-section at the plane of the tetrodes (Metal components of the tetrodes and Microdrive are black in the inverse CT image). The arrow points to the tetrodes tip. **B.** A 3D high resolution MRI scan of a barn owl's brain was aligned and scaled to fit the 3D CT image (see SI Appendix). The image in B shows the aligned MRI image at the plane of the tetrode. Superimpose on the MRI image is the transparent CT image in A. The tetrode track is designated by a yellow line. The arrow points to the lateral tip of the lateral ventricle, the ventricle is the bright line in the MRI image, above it and lateral to it is the Hp. **C-D.** Estimation of the tetrode track in an owl implanted with tetrodes in HA_p. Images are plotted similarly to A and B. Note the tetrode track is lateral from the tip of the lateral ventricle (marked by the arrow in D). Neural data from this owl are not presented in the current paper, but stereotaxic coordinates used in the implantation surgery are the same as used here for targeting HA_p. Significant place cells were recorded from both owls.

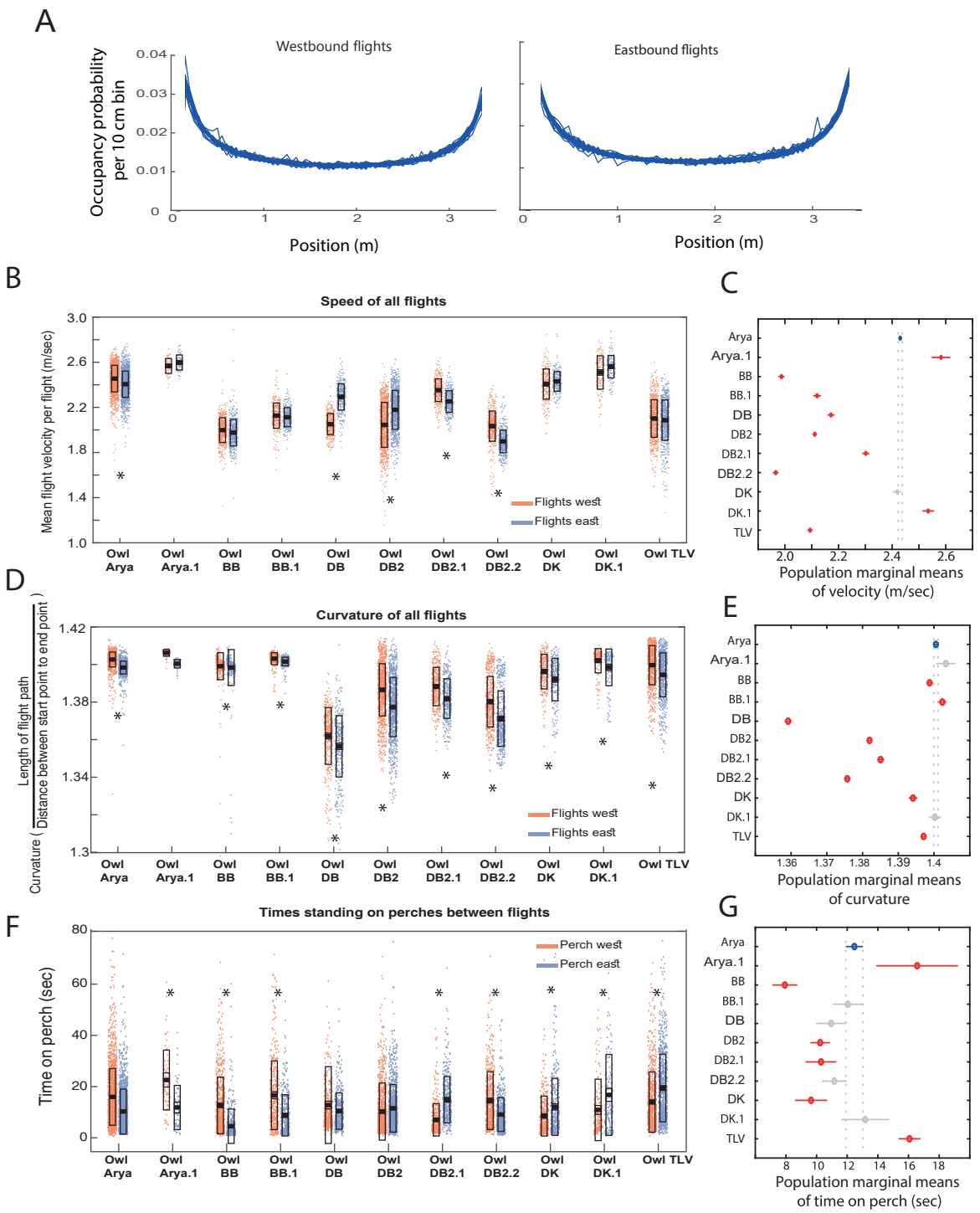

Figure S3. Owls' flight behavior. **A.** Occupancy probability curves (the relative time spent at each 10 cm bin) from 40 different behavioral sessions of the same owl. The curves for westbound flights are shown on the left, and for eastbound flights on the right. The occupancy curves are remarkably similar across flights and directions, following a bell shaped velocity curve. **B.** The mean flight velocity of all flights, separated for all 11 experiments; each experiment is separated to westbound and eastbound flights (red and green respectively). Asterisks indicate experiments in which the mean of flights to west was significantly different from the mean of flights to east (post-hoc Tukey-Kramer multiple comparison test; $p<0.01$). **C.** A graph showing the multiple comparison of the means of the different experiments. Shown for each experiment is the mean and the comparison interval. If the comparison intervals of two groups do not intersect, they are significantly different from each other (post-hoc Tukey-Kramer multiple comparison test; $p<0.01$). Owl's flights were remarkably stereotypic, hence very small velocity differences can be highly significant between owls and between directions. **D and E.** Same as B and C but for the curvature of all flights. **F and G.** The times spent on the perches in-between flights, shown separately for west perch (red) and east perch (green). Format as in B. **G.** Comparison of the mean time spent on the perch between all 11 experiments. Format as in C.

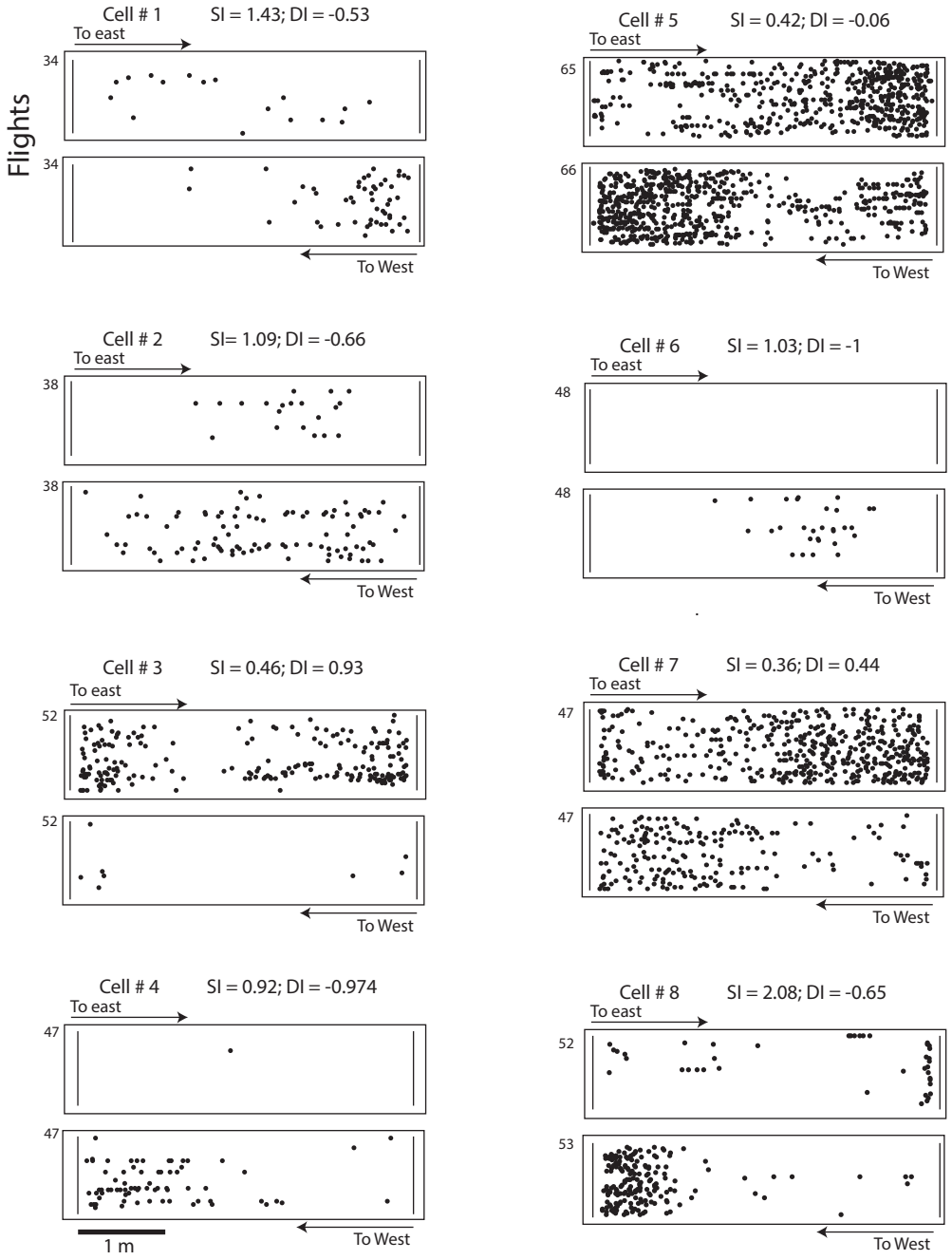

Fig. S4. Examples of 8 place-cells recorded from the hippocampal formation (Hp), showing place tuning and directionality during flight. In each example, the upper raster shows flights to east and the lower raster flights to west. The number of flights in each direction is shown on the y-axis. We indicated above each example the spatial information (SI, in bits/spike) of the direction with the largest value, and the discrimination index (DI) of flight direction.

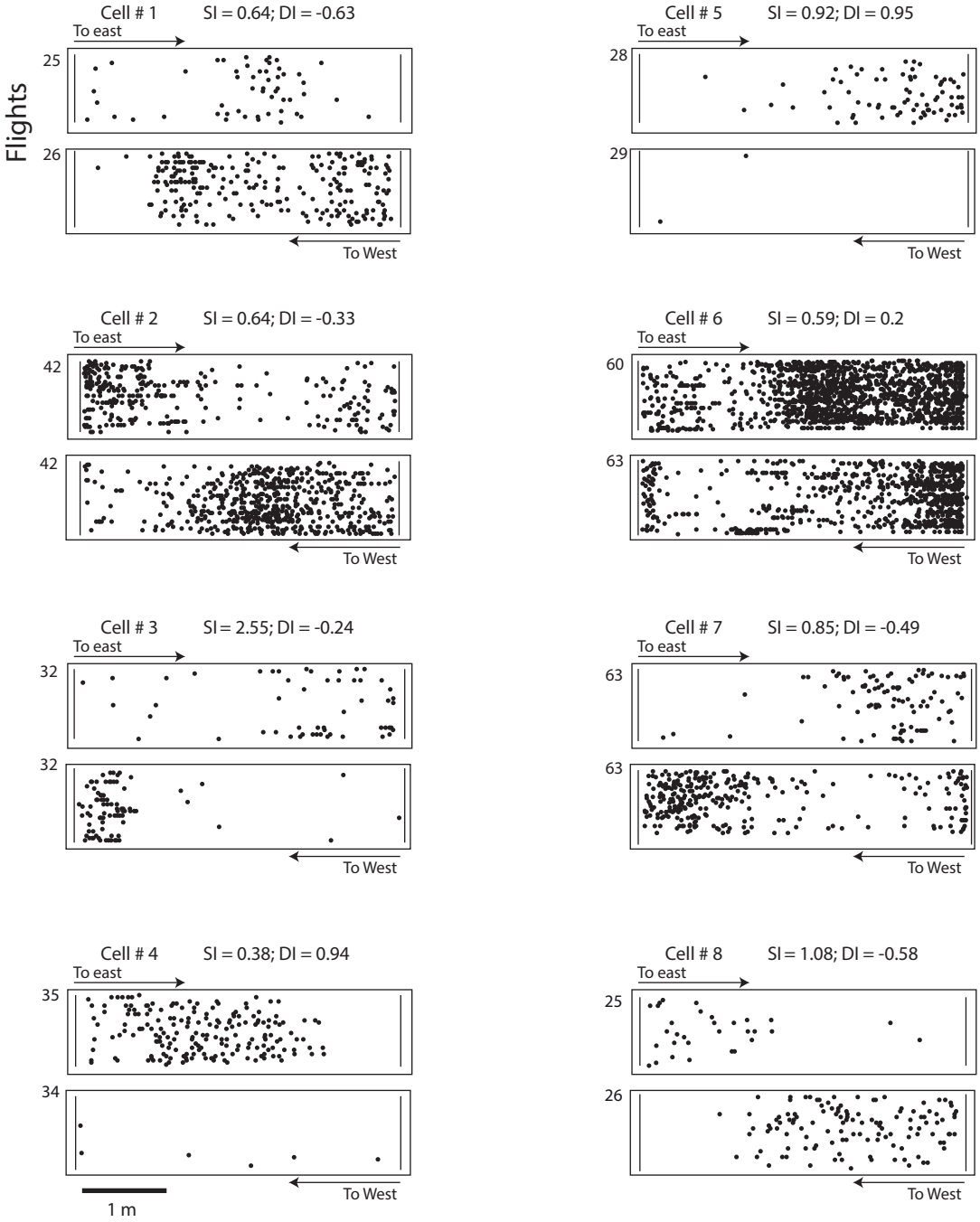

Fig. S5. Examples of 8 place cells recorded from the posterior part of the hyperpallium apicale (HA_p). In each example, the upper raster shows flights to the east and the lower raster flights to the west. The number of flights in each direction is shown on the y-axis. We indicated above each example the spatial information (SI, in bits/spike) of the direction with the largest value, and the discrimination index (DI) of flight direction.

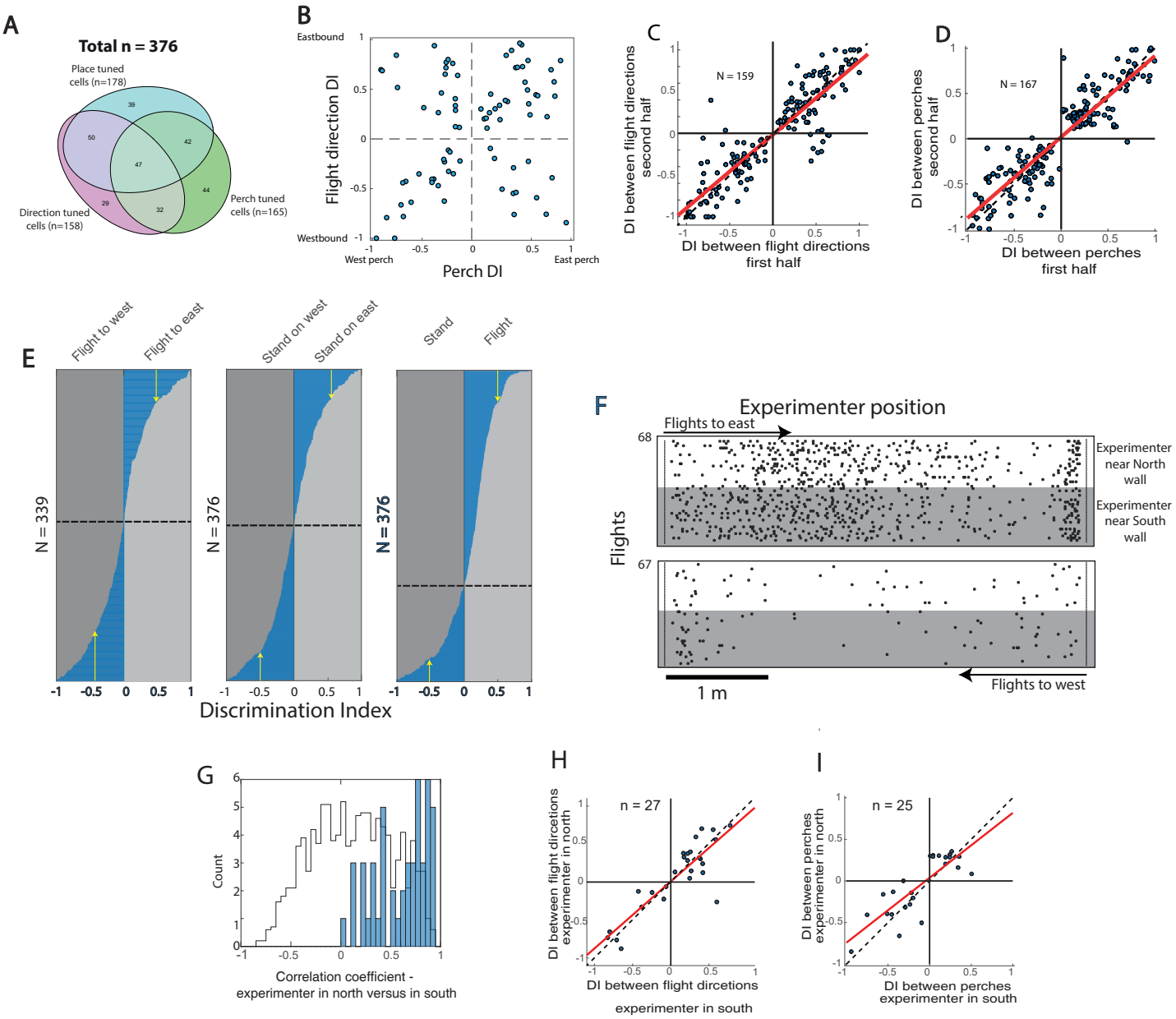

Fig. S6. **A.** Venn-diagram showing the relations between three types of spatial modulations (place-tuning during flight, direction selectivity, and perch selectivity) in the population of neurons from the HA_p. **B**. Scatterplot showing the relationship, within cells, between the perch discrimination index (DI) and the flight-direction discrimination index (DI). Plotted as in Fig. 2C. **C.** Discrimination indices between flight directions, for the first half of the session versus the second half of the session. Only cells that significantly discriminated between flight directions were included in this graph. Dashed line, identity-diagonal; red line, linear-regression. **D**. Same as in D, but showing the discrimination indices between perches, in the first half versus second half of the session. **E.** Histograms showing the discrimination indices (DI) of all cells recorded in the HA_p. Cells were sorted along the y-axis, from the most negative to the most positive DI. The horizontal dashed line indicates the zero DI. The number of cells in each graph is shown on the left. Vertical arrows mark cells with DI > 0.5 in both directions. **F**. Raster plots of an example neuron recorded in a session during which the experimenter switched sides in the middle of the session: the experimenter stood first adjacent to the south wall and later adjacent to the north wall. Gray areas in the raster mark the trials in which the experimenter was in the south, and white areas – in the north. **G-I.** Graphs showing the Pearson correlations between 1D firing-rate maps when the experimenter was in the south versus north (G), the discrimination indices between flight-directions when the experimenter was in the south versus north (H), and the discrimination indices between perches when the experimenter was in the south versus north (I).

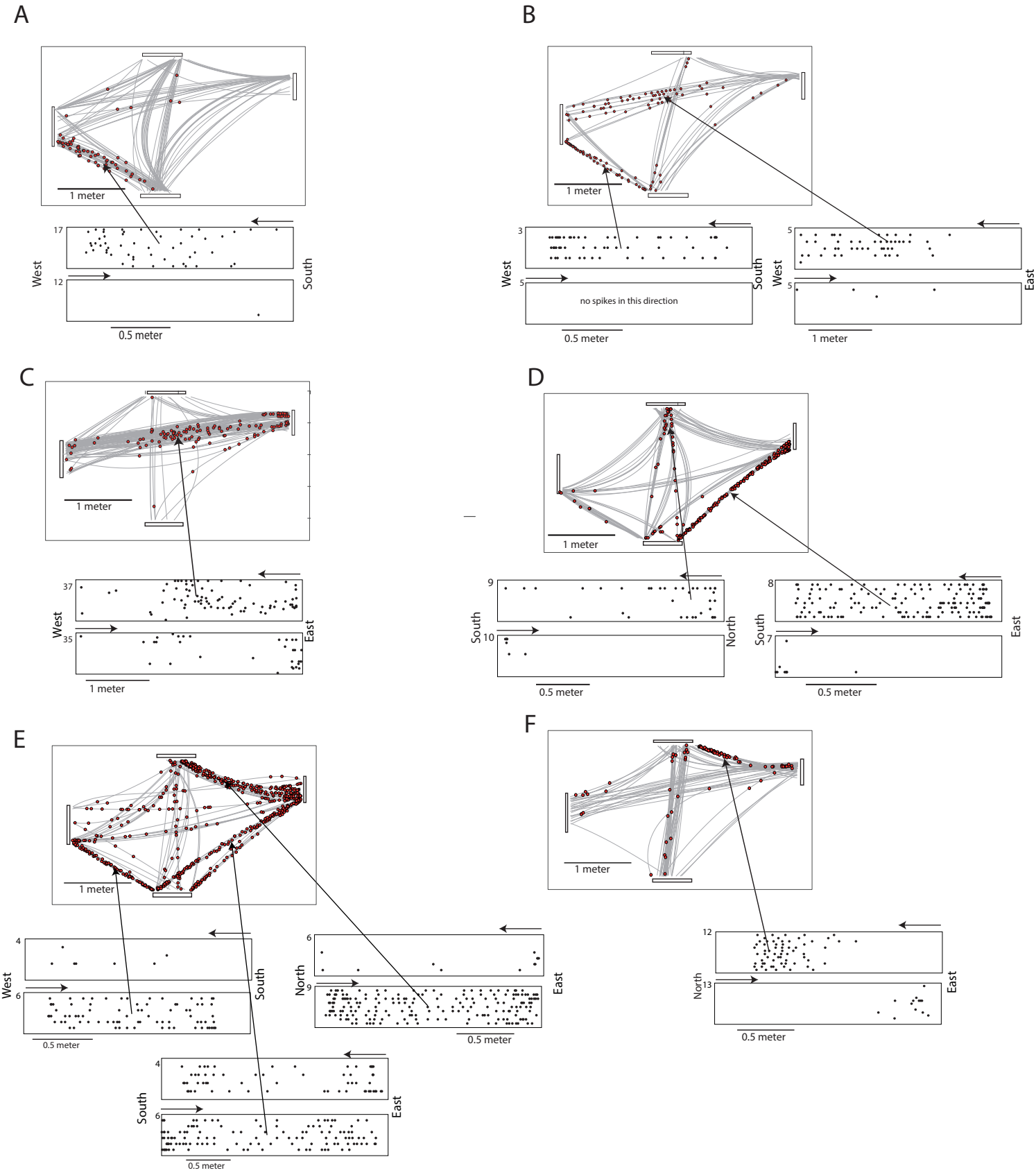

F**ig. S7.** Examples of 6 cells recorded in the Hp during the feeder task. **A.** Data from a single neuron is shown. Left panel shows a 2D upper view of the flight paths (grey lines). Perches are designated by the black rectangles. Upper perch is north. Red dots designate the occurrences of action potentials. Only spikes during flight are shown. The raster plots below, show the occurrences of spikes in the south-west flights, separately for each direction. **B-F.** same as in A but showing results from different neurons. The arrows in all panels connect the position of spike occurrences in the 1D flight path with the corresponding position in the 2D flight graph above. Only flight paths with substantial firing relative to other flight paths are shown in raster format.

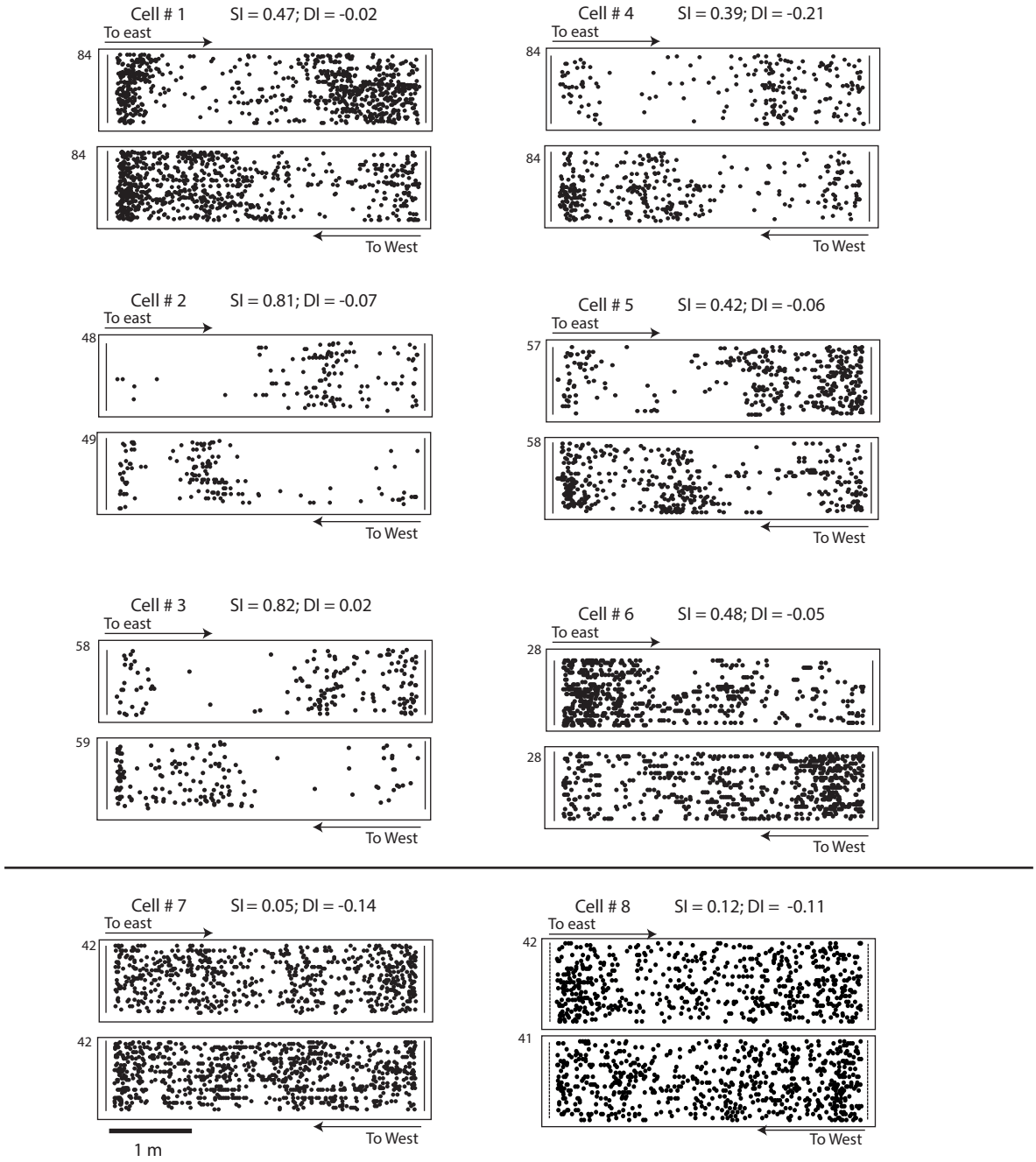

Fig. S8. Examples of 8 cells recorded from visual Wulst. The number of flights in each direction is shown on the y-axis. We indicated above each example the spatial information (SI, in bits/spike) of the direction with the largest value, and the discrimination index (DI) of flight direction. Cells shown above the horizontal line are place-cells (SI is significant compared to shuffles and SI > 0.3). Cell #7 and #8 are examples of cells which are significantly spatially modulated ($p<0.01$; circular shuffling) but the SI is smaller than 0.3.

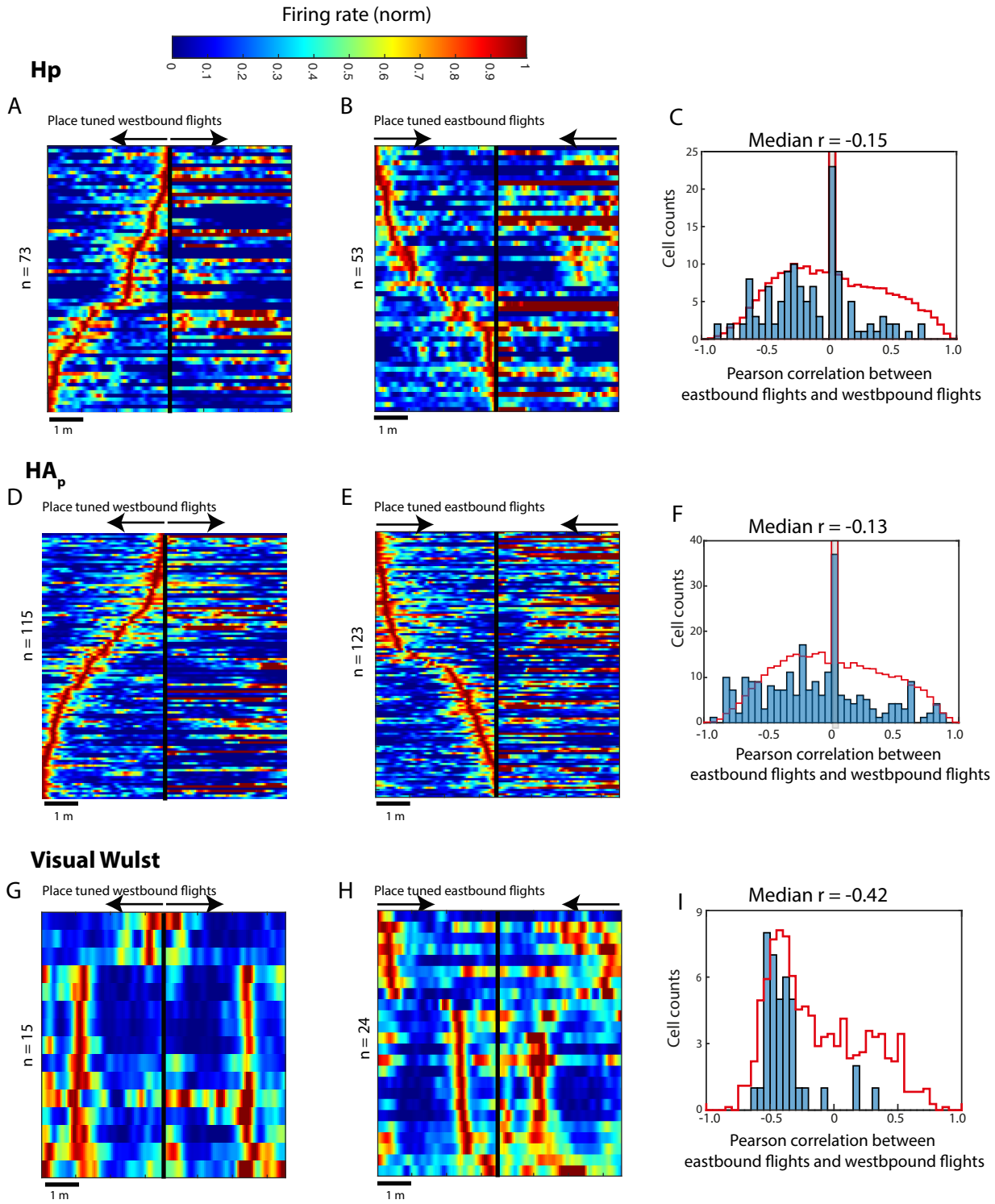

Fig. S9. Comparison between eastbound rate-maps and westbound rate-maps. **A.** All place-cells in Hp, which are place-tuned in westbound flights, are shown and sorted according to the position of peak firing-rate from the onset of flight. Each line shows the normalized rate-maps of one cell in both directions. The black vertical line separates westbound directions (significantly tuned and sorted) from eastbound directions of the same cells. The arrows show the onset and direction of flight. **B.** Shows the same as A, but for all place-cells in Hp, which were place-tuned in eastbound flights. Arrows show the onset and direction of flight. **C.** The blue histogram shows the distribution of the Pearson correlations between all spatially tuned rate maps, in the Hp, with the corresponding (same cells) rate maps in the opposite direction. The red curve is the cell-shuffled distribution of the Pearson correlations of all spatially tuned rate-maps with all rate-maps from the other cells in the opposite direction. Cells in which no spikes were fired in one of the directions were registered as zero correlation. Hence, the large bar at zero (light gray bar). **D-F.** Results from all place cells in HA_p, plotted and analyzed similar to A-C. **G-I.** Results from all place cells in visual Wulst, plotted and analyzed similar to A-C. In visual Wulst (panels G and H), a clear mirror image appears in the corresponding opposite direction – suggesting that visual Wulst neurons primarily fire as a function of distance from takeoff, similarly in both directions. In all three areas, the distribution of the Pearson correlations between the two directions of the real cells (blue bars in panels C, F and G) is significantly shifted towards negative correlations (Kolmogorov-Smirnov test, $p<0.001$); notably, the effect in visual Wulst is substantially larger.

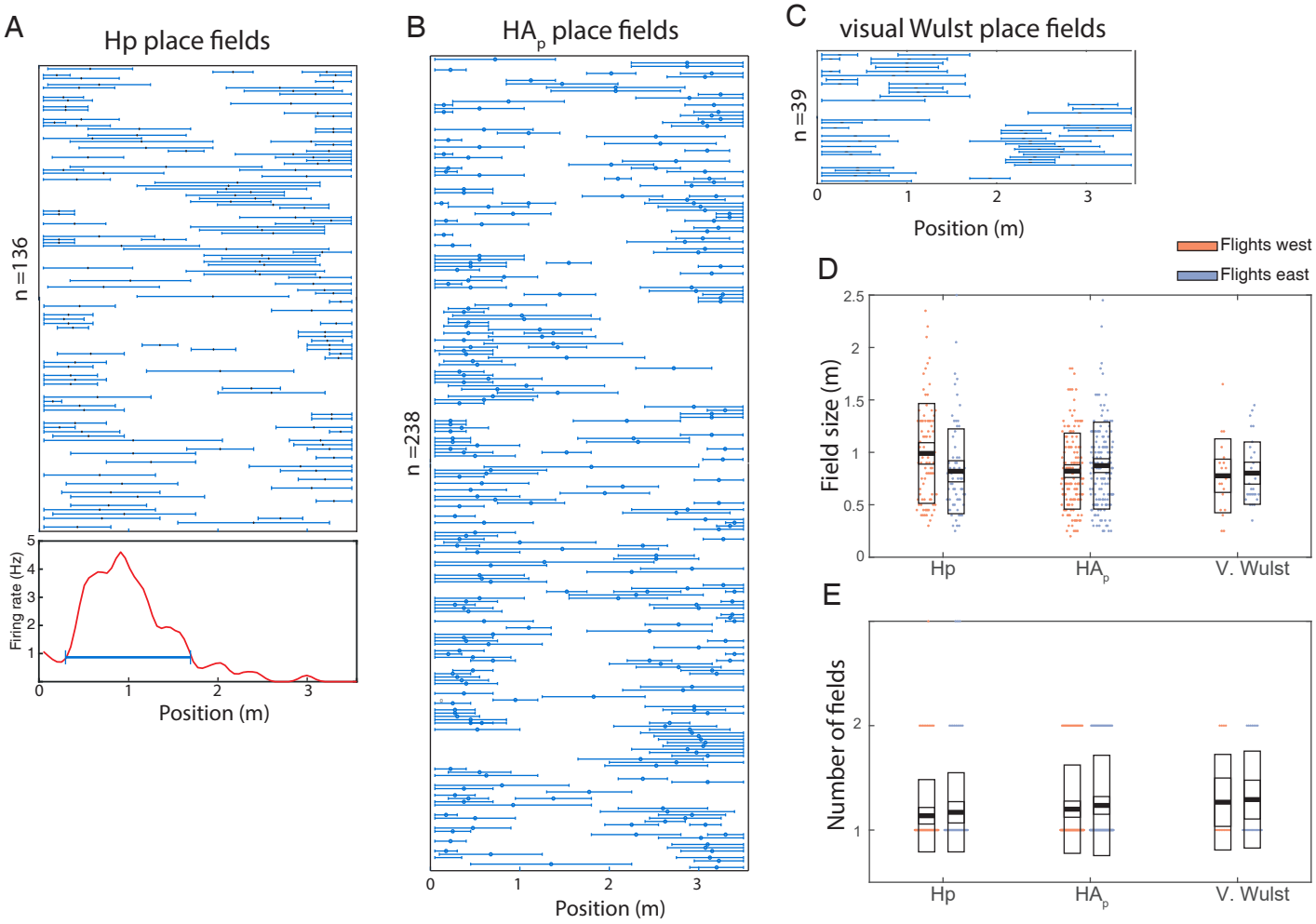

Fig. S10. Analysis of place field size and number of place fields per direction. **A.** Place fields (blue horizontal lines), computed from all significant place-tuned firing rate maps in the Hp. Each line is a single cell (n=136). Place fields were defined as the intervals covering firing rates that are more than 20 % of the main peaks in significant place-tuned firing rate maps (see Methods). Example of a place field (blue horizontal line) superimposed on the corresponding rate map (red line) is shown in A (bottom). **B.** Place fields, computed from all significant place-tuned firing rate maps in the HA_p (n=238). Format as in A. **C.** Place fields (blue horizontal lines), computed from all significant place-tuned firing rate maps in visual Wulst (n=39). **D.** Dots show all place field sizes, separated for Hp, HA_p and visual Wulst, as well as for flight direction. The dark bars designate the means and the box the STD and SEM. Mean field size is not significantly different between the areas nor the directions (2-way ANOVA; main effect of area, $p = 0.17$; main effect of direction, $p = 0.52$). **E.** The number of place fields in the rate maps, shown for the different brain areas and the flight directions. Fields varied between 1 and 2 fields per rate map. The dark bars show the mean values. The distribution of field numbers were not significantly different between the brain areas (Kruskal-Wallis test; $p=0.17$).

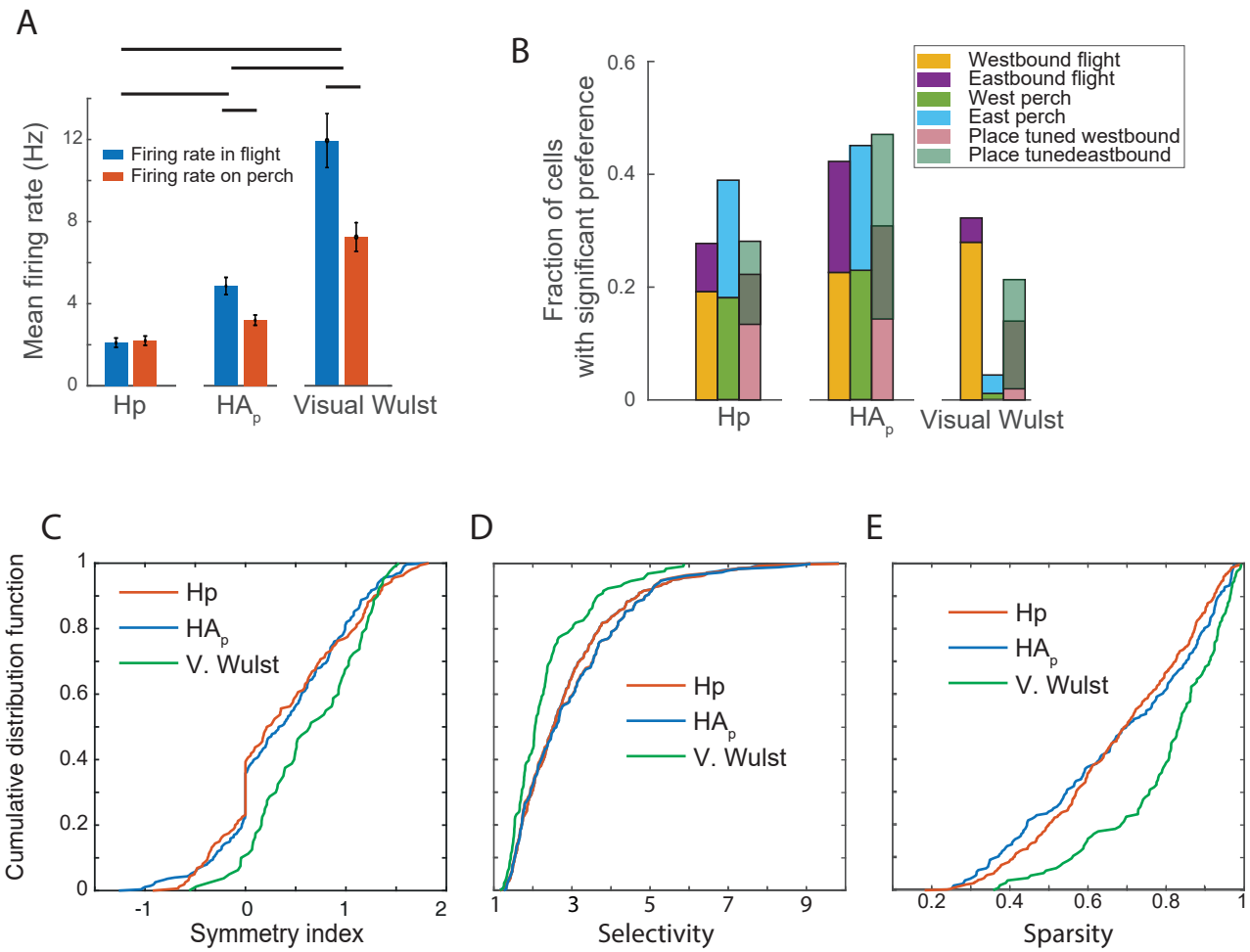

Fig. S11. Comparison between the different brain areas. **A.** Comparison between the mean firing-rates of all the neurons recorded in Hp, HAp and Wulst, separately for firing-rates during flight (blue) and firing rates when standing on the perch (red). Error bars are SEM. Horizontal lines above the bars indicate $p < 0.01$ (t-test). **B.** Comparison between the fractions of cells in Hp, HAp and Wulst that significantly ($p < 0.01$) preferred flights to east versus flights to west; significantly preferred the east perch versus the west perch; and the fraction of place-cells during westbound flights, eastbound flights or both. **C.** Cumulative distributions of the symmetry indices from all cell that where significantly modulated by location ($p < 0.01$) in the three brain regions, including cells with SI values smaller than 0.3. Symmetry indices were significantly smaller in Hp and in HAp as compared to visual Wulst (Kolmogorov-Smirnov test, $p<0.001$). **D-E.** Comparison between the different brain regions of the cumulative distribution functions of two common spatial metrics: (1) Selectivity - the maximum firing rate divided by the mean firing rate. (2) Sparsity - $\frac{(\sum p_i f_i)^2}{\sum (p_i f_i)^2}$ where P_i is the occupancy probability of bin i and f_i is the firing rate of bin i. In both metrics the spatial representations were significantly narrower in Hp and in HAp as compared to visual Wulst (Kolmogorov-Smirnov test, $p<0.001$).

Table S1: The location of recordings, the number of sessions, and the number of cells recorded in each of the experiments and in each of the categories.

2-perch experiments	Owl name	Brain location of tetrodes	# Sessions	# Single Units	Place tuning during West flights	Place tuning During East flights	Flight West pref. Cells	Flight East pref. Cells	Perch West pref. Cells	Perch East pref. Cells
1	Owl Arya	Left Hp	40	220	38	30	39	13	30	35
2	Owl Arya	Right Hp	4	7	0	0	0	0	1	0
3	Owl DK	Left Hp	8	12	4	1	4	2	7	0
4	Owl DK	Right Hp	4	14	2	0	0	8	1	7
5	Owl DB2	Right Hp	16	38	16	14	13	3	13	14
6	Owl BB	Right Hp	11	61	13	8	24	11	20	16
	Total Hp		**83**	**352**	**73**	**53**	**80**	**37**	**72**	**72**
6	Owl DB	Left HAp	13	49	19	17	8	8	11	9
7	Owl DB2	Left HAp	25	152	42	45	31	33	41	28
8	Owl TLV1	Right HAp	22	175	56	63	46	32	33	44
	Total HA_p		**60**	**376**	**117**	**125**	**85**	**73**	**84**	**81**
9	Owl DB2	Left V.Wulst	9	47	4	7	17	3	0	0
10	Owl BB	Right V.Wulst	10	46	11	17	9	1	1	3
	Total V. Wulst		**19**	**93**	**15**	**24**	**26**	**4**	**1**	**3**
4-perch feeder experiments		Brain location of tetrodes	# sessions	# single units	# place-cells	# perch cells	-	-	-	-
11	Owl BB	Right Hp	59	169	45	60				
12	Owl Waldo	Left Hp	17	104	42	26				
13	Owl DB2	Right Hp	22	37	6	6				
	Total 4-perch experiments		**98**	**310**	**93**	**92**	-	-	-	-

Table S2: Comparison of results between the left and right hemispheres. Grey columns show numbers of neurons recorded in the left hemisphere and white columns indicate numbers of neurons recorded in the right hemisphere.

Brain Area	Brain Hemisphere	# Sessions	# Single Units	Place Tuning During West flights	Place Tuning During West flights	Flight West pref. Cells	Flight East pref. Cells	Perch West pref. Cells	Perch East pref. Cells
Hp	Left	48	232	42	31	43	15	37	35
	Right	35	120	31	22	37	22	35	37
HA_p	Left	38	201	61	62	39	41	52	37
	Right	22	175	56	63	46	32	33	44
Visual Wulst	Left	9	47	4	7	17	3	0	0
	Right	10	46	11	17	9	1	1	3
Overall	Left	95	480	107	100	99	59	89	72
	Right	67	341	98	102	92	55	69	84

Table S3: Percent place cells based on different spike isolation criteria. The percentage of place cells has been extracted per each brain area using three different combinations of criteria for single unit isolation: Upper threshold of L-ratio, Lower threshold of Isolation Distance. For comparison, the first row shows the numbers of all single units without an L_ratio/isolation-distance thresholds.

L-Ratio threshold	Isolation Distance threshold	Area Hp			Area HA_p			Visual Wulst			Combined		
		# cells	**# place cells**	**% place cells**	**# cells**	**# place cells**	**% place cells**	**# cells**	**# place cells**	**% place cells**	**# cells**	**# place cells**	**% place cells**
-	-	352	96	27.3	376	178	47.3	93	27	29	821	301	36.6
0.3	10	242	72	29.8	233	109	46.8	54	16	29.6	529	197	37.2
0.2	15	201	60	29.8	200	93	46.5	43	13	30.2	444	166	37.4
0.1	30	97	26	26.8	104	39	37.5	13	1	7.7	214	66	30.8

Movie 1 Legends: Two flights are shown in slow motion. One from the east to the west and one from the west to east. Spikes occurrences during flight are audible. The video camera is sensitive to near IR thus the reflectors on the owl's head and the light from the cameras are clearly visible in the video but are barely visible by the owl.

Movie 2 Legend: A video showing the 2D flight path in an example 2-perch experiment. Blue lines designate flights to west and green lines flights to east. Red dots designate the firing of action potential of a single neuron recorded in this session. Times on the perches are omitted.

Movie 3 Legend: A video showing the 2D flight path in an example 4-perch feeder experiment. In this example the feeder was positioned on the east perch. The target (rewarding) perch was changed continuously during the experiment. Its temporarily location is marked in the video by the word Target. Time on perches is omitted. The red dots indicate the firing of action potentials.